

An overview of a unified theory of dynamics of vehicle–pavement interaction under moving and stochastic load

Lu Sun

Received: 18 May 2013 / Revised: 12 July 2013 / Accepted: 19 July 2013 / Published online: 26 September 2013
© The Author(s) 2013. This article is published with open access at Springerlink.com

Abstract This article lays out a unified theory for dynamics of vehicle–pavement interaction under moving and stochastic loads. It covers three major aspects of the subject: pavement surface, tire–pavement contact forces, and response of continuum media under moving and stochastic vehicular loads. Under the subject of pavement surface, the spectrum of thermal joints is analyzed using Fourier analysis of periodic function. One-dimensional and two-dimensional random field models of pavement surface are discussed given three different assumptions. Under the subject of tire–pavement contact forces, a vehicle is modeled as a linear system. At a constant speed of travel, random field of pavement surface serves as a stationary stochastic process exciting vehicle vibration, which, in turn, generates contact force at the interface of tire and pavement. The contact forces are analyzed in the time domain and the frequency domains using random vibration theory. It is shown that the contact force can be treated as a nonzero mean stationary process with a normal distribution. Power spectral density of the contact force of a vehicle with walking-beam suspension is simulated as an illustration. Under the subject of response of continuum media under moving and stochastic vehicular loads, both time-domain and frequency-domain analyses are presented for analytic treatment of moving load problem. It is shown that stochastic response of linear continuum media subject

to a moving stationary load is a nonstationary process. Such a nonstationary stochastic process can be converted to a stationary stochastic process in a follow-up moving coordinate.

Keywords Vehicle–pavement interaction · Random field · Continuum medium · Spectral analysis · Green’s function · Linear system

List of Symbols

$\mathbf{F}(\mathbf{x}, t)$	Moving source
$\delta(\cdot)$	Dirac delta function
v	Source velocity
$P(t)$	Source magnitude
$\mathbf{h}[\cdot]$	Impulse response function
$\mathbf{H}[\cdot]$	Frequency response function
$S(\cdot)$	Power spectral density
$R(\cdot)$	Correlation function
$E[\cdot]$	Expectation
σ^2	Variance
ψ	Standard deviation
$\mathbf{G}[\cdot]$	Green’s function
$\mathbf{u}[\cdot]$	Response function of continuum media

1 Introduction

The investment of the United States in the nation’s transportation infrastructure alone (highways, bridges, railways, and airports) amounted to \$7 trillion by 1999. To preserve infrastructure longevity in a cost-effective manner, the research in pavement design and infrastructure management has been growing rapidly in recent years. From a pavement design point of view, pavement response, damage, and performance are essentially the result of long-term

L. Sun (✉)
Department of Civil Engineering, The Catholic University
of America, Washington, DC 20064, USA
e-mail: sunl@cua.edu

L. Sun
International Institute of Safe, Intelligent and Sustainable
Transportation & Infrastructure, Southeast University,
Nanjing 210096, China

vehicle–pavement interaction. When vehicle speed is low, the dynamic effect of vehicular loads on pavements is insignificant. However, with the promotion of high-speed surface transportation in the world, this dynamic effect must be taken into account to develop more rational pavement design methods. For instance, real causative mechanisms that lead to fatigue damage of pavement material might be frequency dependent. From an infrastructure management point of view, vehicle–pavement interaction has a profound impact on the way that existing technologies of structural health monitoring, environmental vibration mitigation, nondestructive testing and evaluation, and vehicle weight-in-motion are to be improved, innovated and implemented. For instance, modern high-speed surface transportation systems are normally accompanied by rises in levels of noise and vibration that may cause a significant detrimental effect to the ecology. Vehicle–pavement interaction-induced structure-borne and ground-borne vibrations emit and propagate toward some extent. Residents may experience hardship from uncomfortable vibration, and high-precision equipment may suffer from malfunctioning to irreparable damage. To mitigate noise and vibration in surrounding areas of roadway, it is necessary to investigate predominant frequencies of vehicle–pavement interaction, the source of vibration, so as to develop effective noise and vibration countermeasures. The study of vehicle–pavement interaction also plays a critical role in developing better inversion algorithms for nondestructive testing and evaluation of transportation infrastructure. In addition, taking into account dynamic effects of vehicle vibration caused by rough surface may considerably improve accuracy and reliability of weigh-in-motion systems, which measure a vehicle's weight as it travels at a normal speed.

Vehicle–pavement interaction is not only a central problem to pavement design, but also has a profound impact on infrastructure management, vehicle suspension design, and transportation economy. Figure 1 shows a central role of vehicle–pavement interaction played in a wide variety of applications. From a vehicle-design point of view, a designer needs to consider vehicle vibration and controllability, which affect ride quality and vehicle maneuver. Vehicle–pavement interaction also has a huge economic impact. As pavement performance deteriorates and roadway surface gets rougher, both operation costs (fuel, tire wear, and routine maintenance) and roadway maintenance cost of the vehicle increase dramatically, accompanied by decreasing transportation productivity. There is no doubt that there is a great and urgent need for fundamental research on vehicle–pavement interaction due to rapid deterioration of huge highway infrastructure nationwide, tight maintenance budget, and the key role played by vehicle–pavement interaction.

Since the American Association of State Highway Officials (AASHO) road test, the fourth power law has been widely used by pavement engineers to design highway and airfield pavement and to predict the remained life and cumulated damage of pavements [1–3]. Besides the damage caused by static loads, dynamic loads may lead to additional pavement damage. A consequence of a high power in the damage law is that any fluctuation of pavement loading may cause a significant increase in the damage suffered by pavement structures. A number of recent filed measurements and theoretical investigations showed that vehicle vibration-induced pavement loads are moving stochastic loads [4–8]. The researchers concluded that vibrations of vehicles were related primarily to pavement surface roughness, vehicle velocity, and suspension types [9–13].

Estimation of pavement damage caused by dynamic loads varies anywhere from 20 % to 400 % [14]. The smaller estimates are based on the assumption that peak dynamic loads (and hence the resulting pavement damage) are distributed randomly over the pavement surface. The larger estimates are based on the assumption that vehicles consistently apply their peak wheel loads in the same areas of the pavement. Theoretical studies by Cole [15] and Hardy and Cebon [16] confirmed that for typical highway traffic, certain areas of the pavement surface always suffered the largest wheel forces, even when the vehicles had a wide range of different suspension systems, payloads, and speeds.

Complicated relationships exist among vehicle suspension, dynamic wheel loads, pavement response, and damage [17–19]. On one hand, it has been known for years on how to manufacture automobiles operating properly on a variety of pavement surfaces. On the other hand, however, the effect of vehicle design on pavement has not been thoroughly studied. For instance, Orr [20] stated in his study that comparatively little was known about the influence of suspension design on pavement in the automobile industry yet.

A number of obstacles exist in revealing vehicle–pavement interaction. A theoretical foundation universally applicable to the involved specific problems is no doubt very attractive. It will not only provide a guide for experimental study and validation, but will also enable better design and maintenance of vehicles and pavements. As such, this article provides an overview of a unified theory for dynamics of vehicle–pavement interaction under moving and stochastic loads. This article covers three major aspects of the subject: pavement surface, tire–pavement contact forces, and response of continuum media under moving and stochastic vehicular loads developed by Sun and his associates (Fig. 2). The remainder of this article is organized as follows. Section 2 addresses mathematical

description of pavement surface roughness. Section 3 studies contact force generated due to vehicle–pavement interaction, which is the source to both vehicle dynamics and pavement dynamics. Section 4 investigates pavement response under moving stochastic loads. Section 5 discusses difficulties and deficiencies in the existing research, and projects further research and applications. Section 6 makes concluding remarks.

2 Pavement surface

Irregularities in pavement surface are often called roughness. All pavement surfaces have some irregularities. The National Cooperative Highway Research Program defines “roughness” as “the deviations of a pavement surface from a true planar surface with characteristic dimensions that affect vehicle dynamics, ride quality, and dynamic pavement loads [21].” Factors contributing to roughness, in a general sense, include vertical alignment, cracks, joints, potholes, patches and other surface distresses.

Newly constructed pavements may be poorly finished or have design features such as construction joints and thermal expansion joints, which can be main sources of vehicle vibration [22, 23]. Measurements show that pavement roughness can be modeled as a random field consisting of different wavelength. Considerable effort has been devoted to describing pavement surface roughness [24–26]. The

peak-to-valley measurements, the average deviation from a straight edge, and the cockpit acceleration are several distinct approaches that have been suggested for pavement surface characterization [27]. Practical limitations of these three approaches could be found in the study of Hsueh and Penzien [28].

Spectrum of a deterministic function referring to its Fourier transform reveals sinusoid components that a deterministic periodic or nonperiodic function is composed of. Spectrum analysis of a deterministic function $f(t)$ can be obtained if and only if this deterministic function satisfies Dirichlet condition and absolute integrability condition [29]:

$$\int_{-\infty}^{\infty} |f(t)| dt < +\infty. \tag{1}$$

Pavement surface as a random field of elevation does not decay as spatial coordinates extend to infinity; therefore, it does not satisfy inequality (1). For this reason, taking Fourier analysis to a sampled pavement surface does not make too much sense in theory. However, the correlation vector of random field does decay as spatial coordinates extend to infinity. Hence, applying Fourier transform to correlation vector of pavement surface, commonly known as power spectral density, does serve the purpose of spectrum analysis in theory [30]. As such, mathematical description of pavement surface takes place under the theoretical framework of spectral analysis of stochastic process.

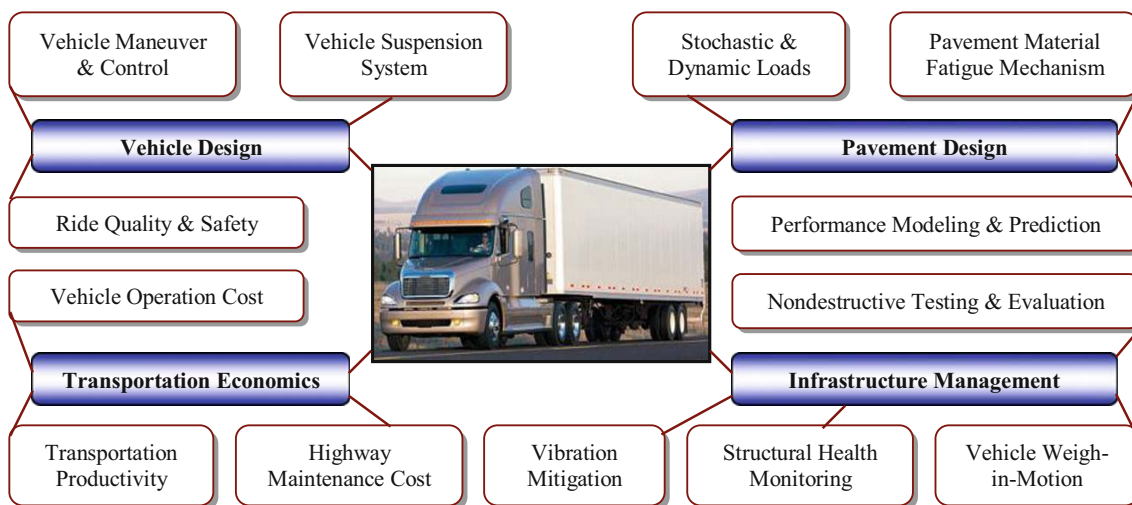


Fig. 1 A central role of vehicle–pavement interaction played in various applications

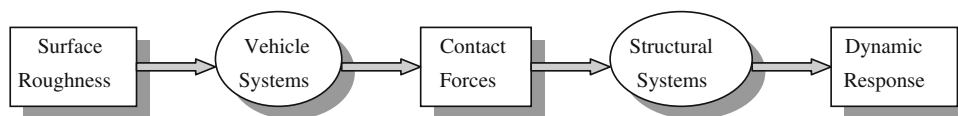


Fig. 2 Dynamics of vehicle–pavement interaction

The following subsections consist of a general mathematical framework for describing pavement surface roughness, a review of statistical description of pavement surface roughness, a description of periodic joints of cement concrete pavement, and three different hypotheses when projecting a one-dimensional road profile to a two-dimensional pavement surface.

2.1 One-dimensional description

Given the manifest complexity exhibited in pavement surface as a random field, making some assumptions becomes indispensable to simplify mathematical description of pavement surface. Commonly used assumptions on surface roughness are that surface roughness is an ergodic and homogeneous random field with elevation obeying Gaussian distribution [31–33]. The assumption of ergodicity makes sure that the temporal average of a sample of stochastic process equals to the statistical mean of stochastic process, which enable one to obtain the statistical characteristics of a stochastic process by measuring only a few samples. The assumption of homogeneity ensures random property of surface roughness is independent to the sites measured. When a vehicle travels at a constant speed, a homogeneous random field is converted to a stationary stochastic process. The assumption of Gaussian distribution ensures that transformation of such randomness through a linear system is still Gaussian.

Road profile along longitudinal direction (i.e., direction of travel) is often an exchangeable term of pavement roughness. The simplest model describes the pavement surface as a cylindrical surface defined by a single longitudinal profile $\xi(x)$. Figure 3 shows an illustrative example of road profile. Instead of varying with time, the elevation ξ of the surface varies with respect to longitudinal distance x along the direction of travel. In the spatial domain, low-frequency components correspond to long wavelengths while high frequency components correspond to short wavelengths. Let $\xi(x)$ be a zero mean, homogeneous, Gaussian random field. Its probabilistic structure can be completely described by either the autocorrelation function or the power spectral density (PSD).

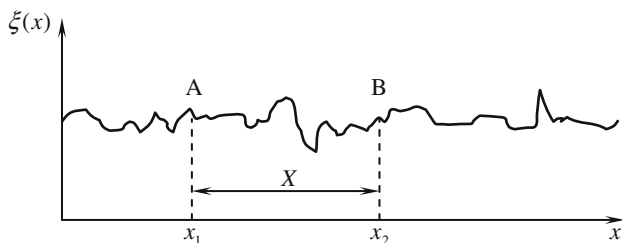


Fig. 3 One-dimensional road profile

According to the Winner–Khinchine theory [31], the following expressions constitute a pair of Fourier transform:

$$S_{\xi\xi}(\Omega) = (2\pi)^{-1} \int_{-\infty}^{\infty} R_{\xi\xi}(X) e^{-i\Omega X} dX, \quad (2a)$$

$$R_{\xi\xi}(X) = \int_{-\infty}^{\infty} S_{\xi\xi}(\Omega) e^{i\Omega X} d\Omega, \quad (2b)$$

where X represents the distance between any two points along the road. Wavenumber spectrum, $S_{\xi\xi}(\Omega)$, is the direct PSD function of wavenumber Ω , which represents spatial frequency defined by $\Omega = 2\pi/\lambda$ where λ is the wavelength of roughness. Under the assumption of homogeneity, spatial autocorrelation function $R_{\xi}(X)$ is defined by

$$R_{\xi\xi}(X) = E[\xi(x_1)\xi(x_2)] = E[\xi(x_1)\xi(x_1 + X)] \quad (3)$$

for any x_1 and X . Here $E[\cdot]$ is the expectation operator and can be calculated by

$$E[\xi(x)] = \lim_{X \rightarrow \infty} \frac{1}{2X} \int_{-X}^X \xi(x) dx. \quad (4)$$

This expectation, differing from statistical mean of a random process, is temporal average of a sample of stochastic process.

2.1.1 PSD roughness

As a one-dimensional random field, roughness can be characterized in the spatial domain and the wavenumber domain. An analytic form of PSD roughness is often desired for theoretical treatment [34, 35]. Spectral analysis of pavement roughness has been the subject of considerable research for years. Many function forms of PSD roughness have been proposed to characterize bridge deck surface [36], rail-track surface [33, 37], and airfield runway surface [24, 38].

Sayers et al. [39, 40] suggested a power function for PSD roughness:

$$S_{\xi\xi}(\Omega) = A\Omega^\alpha. \quad (5)$$

Early studies on PSD of longitudinal profiles of runways and roads are a special case of (5) for $\alpha = -2$ [41–44]. Although power function (5) is convenient for parameter estimation and design purpose, it creates mathematical difficulties at $\Omega = 0$, where $S_{\xi\xi}(\Omega)$ becomes infinite. For this reason, two distinct function forms have been proposed in later studies.

One form is to use rational functions: Sussman [45] for (6), Sussman [45], Snyder and Wormley [46], and Yadav and Nigam [47] for (7), Macvean [48] for (8), Bolotin (1984) for (9), and Gillespie [25, 26] for (10), to name a few.

$$S_{\xi\xi}(\Omega) = \frac{S_0(\Omega^2 + \alpha^2 + \beta^2)}{(\Omega^2 - \alpha^2 + \beta^2)^2 + 4\Omega^2\alpha^2}, \tag{6}$$

$$S_{\xi\xi}(\Omega) = \frac{S_0}{\Omega^2 + \alpha^2}, \tag{7}$$

$$S_{\xi\xi}(\Omega) = \frac{S_0}{(\Omega^2 + \alpha^2)^2}, \tag{8}$$

$$S_{\xi\xi}(\Omega) = \frac{4\sigma^2}{\pi} \frac{\alpha\Omega_0^2}{(\Omega^2 - \Omega_0^2) + 4\alpha^2\Omega^2}, \tag{9}$$

$$S_{\xi\xi}(\Omega) = S_0[1 + \Omega_0^2\Omega^{-2}](2\pi\Omega)^{-2}. \tag{10}$$

Another form is to use piecewise functions. For instance, (11) was suggested by the International Organization for Standardization (ISO) to cover different frequency ranges [49–52].

$$S_{\xi\xi}(\Omega) = \begin{cases} C_{sp}\Omega_a^{-w_1} & \text{for } 0 \leq \Omega \leq \Omega_a \\ C_{sp}\Omega^{-w_2} & \text{for } \Omega_a \leq \Omega \leq \Omega_b, \\ 0 & \text{for } \Omega_b < \Omega \end{cases} \tag{11}$$

where Ω_a represents reference frequency, and Ω_b represents cut-off frequency. Iyengar and Jaiswal [33] provided a similar split power law in the form of (11) for rail-track in which $C_{sp} = 0.001(\text{m}^{-2} \text{cycles/m})$ and $w_1 = w_2 = 3.2$. Marcondes et al. [22, 23] proposed an exponential piecewise function:

$$S_{\xi\xi}(\Omega) = \begin{cases} A_1 \exp(-k\Omega^p) & \text{for } \Omega \leq \Omega_1, \\ A_2(\Omega - \Omega_0)^q & \text{for } \Omega_1 \leq \Omega. \end{cases} \tag{12}$$

In all aforementioned PSD roughness, $A, A_1, A_2, p, q, k, w_1, w_2, C_{sp}, \alpha, \beta, S_0,$ and Ω_0 are the real and positive parameters estimated from field test.

Although various PSD functions have been proposed for fitting the measured PSD roughness, it has been found that most pavement profiles including road surface, runway surface, and rail-track surface exhibit very similar trends of PSD curves. Some researchers have even reduced the PSD curves to only two families: one for rigid (cement concrete pavements), and the other for flexible (asphalt concrete pavements) [25, 26].

2.1.2 Effect of periodic joints of rigid pavement

Thermal expansion joints are commonly set on rigid pavement surface to reduce thermal stress in pavement. Thermal joints of rigid pavement can be a significant source of excitation of vehicle vibration, especially when the joint sealing material gets lost. This could cause undesirable riding qualities at a high speed [43]. Figure 4 shows an idealized rigid pavement surface with periodic joints. An actual rigid pavement surface might be considered as a combination of this periodic profile and a random field.

In the spatial domain, pavement roughness $\xi(x)$ in Fig. 4 can be described by a periodic function within a period $[-d/2, d/2]$.

$$\xi(x) = \begin{cases} 0, & x \in [-d/2, -\Delta/2] \\ c(x), & x \in [-\Delta/2, \Delta/2]. \\ 0, & x \in [\Delta/2, d/2] \end{cases} \tag{13}$$

Here spatial period along the longitudinal direction, d , represents slab length of rigid pavement, Δ and h , respectively, represent maximum width and depth of joint, $c(x)$ is named shape function of joint, which is a symmetrical function and describes the shape of the joint. With this description, pavement roughness $\xi(x)$ becomes an even function with period d .

A period function can be legitimately expanded using Fourier series, which is sometimes called frequency spectrum analysis of periodic function [53]. As such, coefficients of the expanded Fourier series of $\xi(x)$ a_n and b_n ($n = 0, 1, 2, \dots$) are given by

$$a_n = \frac{1}{d/2} \int_{-d/2}^{d/2} \xi(x) \cos \frac{n\pi x}{d/2} dx = \frac{2}{d} \int_{-\Delta/2}^{\Delta/2} c(x) \cos \frac{2n\pi x}{d} dx, \tag{14a}$$

$$b_n = 0, n = 0, 1, 2, \dots \text{ (for } \xi(x) \text{ is an even function).} \tag{14b}$$

Wavenumber spectrum of roughness is thus expressed as

$$S_{\xi\xi}(\Omega_n) = a_n^2 + b_n^2 = \frac{4}{d^2} \left[\int_{-\Delta/2}^{\Delta/2} c(x) \cos \frac{2n\pi x}{d} dx \right]^2, \tag{15a}$$

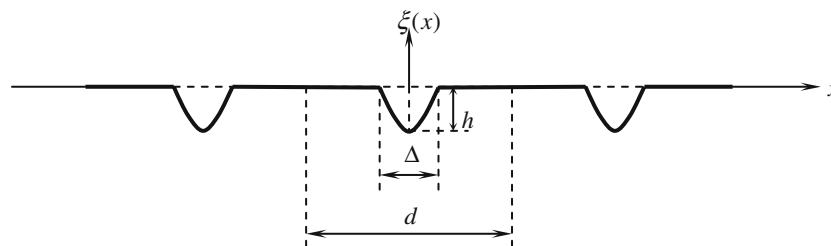


Fig. 4 Periodic joints of rigid pavement surface

$$\Omega_n = n/d \quad (n = 0, 1, 2, \dots) \tag{15b}$$

In which Ω_n represents discrete wavenumber and $S_{\xi\xi}(\Omega_n)$ is discrete wavenumber spectrum. It is evident from (18) that different shapes of joints determine different discrete spatial spectrum. Four types of shape function, namely rectangular curve, parabolic curve, cosine curve, and triangular curve have been observed and investigated by Sun [54].

Table 1 gives the discrete spatial spectrums of these four types of shape functions computed from (15a). The comparison between these discrete spectrums for specified rigid pavement with slab length 5 m and joint width 0.03 m is plotted in Fig. 5 where $S = h\Delta/d$, $\Omega_n = 2\pi n/d$, $n = 0, 1, 2, \dots$, and $\Delta/d = 0.006$. From this figure it can be seen that the spectrum of rectangular joint is the greatest in four types of joints, while the spectrum of triangular joints is the smallest. The ratio of the magnitude of four types of joints based on $S_{\xi\xi}(\Omega_0)$ approximates to 4:1.78:1.62:1. Because $S^2 = (h\Delta/d)^2$, the effect of joint of rigid pavement with long slab length d is much less than that of the pavement with short slab length.

2.2 Two-dimensional description

One-dimensional random field model of pavement surface is adequate for two-wheel vehicles, such as bicycles and

motor-cycles but inadequate for cars and trucks having two or more wheel per axle. Actual highway and airfield pavement consists of a two-dimensional surface of finite width, a nominal camber and grader. The elevation of pavement surface exhibit random fluctuations about the nominal geometry and therefore should be more accurately treated as a two-dimensional random field, $\xi(x, y)$, with space coordinates x and y as the indexing parameters as shown in Fig. 6.

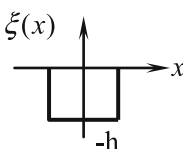
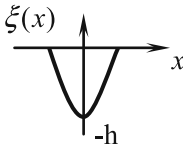
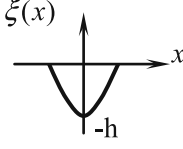
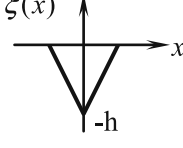
When ignoring those isolated large fluctuations such as potholes, fluctuations of pavement surface can be approximate by a homogenous, Gaussian random field with a zero mean [49, 55]. Probabilistic structure of a two-dimensional random field can be completely defined either by two-dimensional autocorrelation function

$$R_{AC}(X, Y) = E[\xi(x_1, y_1)\xi(x_2, y_2)] = E[\xi(x_1, y_1)\xi(x_1 + X, y_1 + Y)] \tag{16}$$

or by two-dimensional PSD, $S_{\xi\xi}(\Omega, K)$, where $X = x_2 - x_1$, $Y = y_2 - y_1$, Ω and K represent wavenumber in x -axis and y -axis directions, respectively. Here $S_{\xi\xi}(\Omega, K)$ is defined as a double-sided Fourier transform of autocorrelation function (16).

$$S(\Omega, K) = (2\pi)^{-2} \int_{-\infty}^{\infty} \int_{-\infty}^{\infty} R(X, Y) e^{-i(\Omega X + KY)} dX dY. \tag{17}$$

Table 1 Discrete wavenumber spectrum resulting from periodic joints of rigid pavement

Joints	Shape function	Diagram	Discrete spatial spectrum
Rectangular curve	$-h$		$S_{\xi\xi}(\Omega_0) = 4S^2$ $S_{\xi\xi}(\Omega_n) = \left[\frac{\sin(\Delta\Omega_n/2)}{\Delta\Omega_n/2}\right]^2 S_{\xi\xi}(\Omega_0).$
Parabolic curve	$\frac{4h}{\Delta^2}x^2 - h$		$S_{\xi\xi}(\Omega_0) = 16S^2/9$ $S_{\xi\xi}(\Omega_n) = \frac{9[\cos(\Delta\Omega_n/2) - \sin(\Delta\Omega_n/2)/(\Delta\Omega_n/2)]^2}{(\Delta\Omega_n/2)^4} S_{\xi\xi}(\Omega_0).$
Cosine curve	$-h \cos \frac{\pi}{\Delta}x$		$S_{\xi\xi}(\Omega_0) = 16S^2/\pi^2$ $S_{\xi\xi}(\Omega_n) = \left[\frac{\cos(\Delta\Omega_n/2)}{1 - (\Delta\Omega_n/\pi)^2}\right]^2 S_{\xi\xi}(\Omega_0).$
Triangular curve	$\frac{2h}{\Delta} x - h$		$S_{\xi\xi}(\Omega_0) = S^2$ $S_{\xi\xi}(\Omega_n) = \frac{4[1 - \cos(\Delta\Omega_n/2)]^2}{(\Delta\Omega_n/2)^4} S_{\xi\xi}(\Omega_0).$

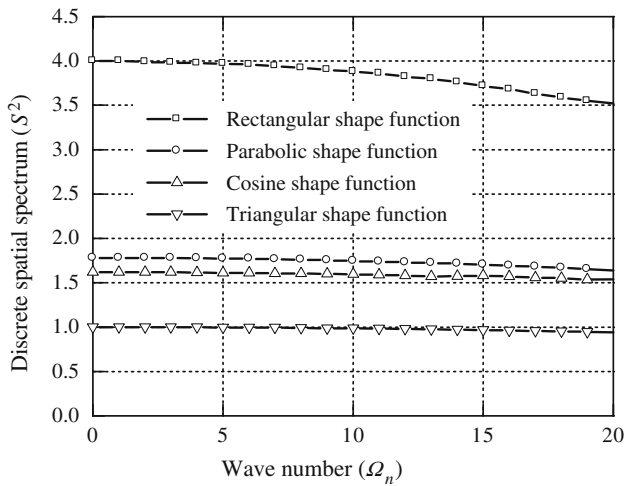


Fig. 5 Discrete wavenumber spectrum resulting from periodic joints of rigid pavement

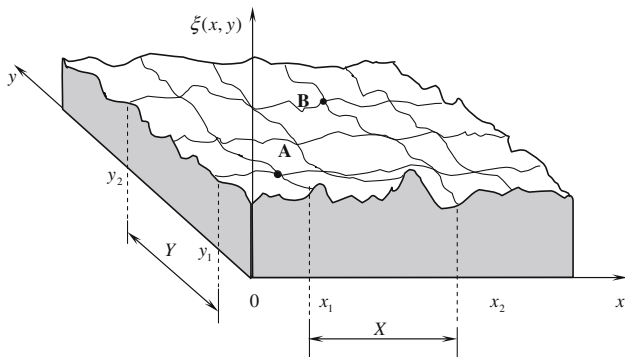


Fig. 6 Two-dimensional random field model of pavement surface

The determination of the two-dimensional autocorrelation function or two-dimensional PSD relies on the measured elevation of the entire pavement surface, which is a possible but formidable task in data acquisition, numerical computation and data storage for hundreds of thousands of miles of roadways. Efforts have, therefore, been made to simplify the two-dimensional random field such that it can be uniquely generated from the one-dimensional random field models by imposing certain hypothetic properties to pavement surface [49, 50, 55].

2.2.1 The hypothesis of isotropy

Consider a two-dimensional random field model of pavement surface as shown in Fig. 7. There are two parallel wheel paths separated by a constant distance Y along the transverse direction. Longitudinal profiles along each wheel path can be derived from the two-dimensional random field $\xi(x, y)$ as follows.

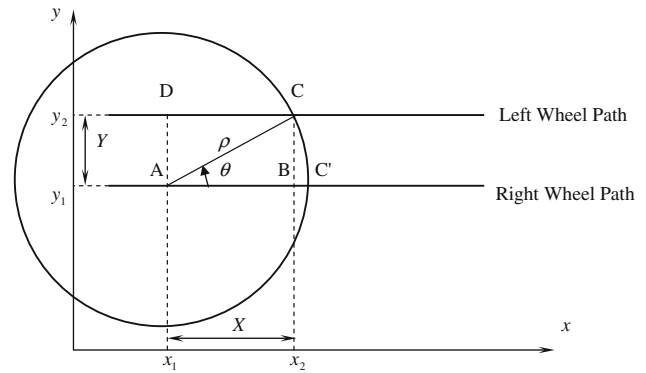


Fig. 7 A plane view of two-dimensional isotropic random field

From (16) the autocorrelation functions between A and B and between D and C are, respectively, given by

$$R_{AB}(X, 0) = E[\xi(x_1, y_1)\xi(x_1 + X, y_1)] \tag{18a}$$

and

$$R_{DC}(X, 0) = E[\xi(x_1, y_2)\xi(x_1 + X, y_2)]. \tag{18b}$$

Since $\xi(x, y)$ is homogenous,

$$R_{AB}(X, 0) = R_{DC}(X, 0) = R_{\xi\xi}(X). \tag{19}$$

Crosscorrelation functions, $R_{AC}(X, Y)$ and $R_{CA}(X, Y)$, are even functions of X and Y :

$$R_{AC}(X, Y) = R_{CA}(X, -Y) = R_{AC}(-X, Y). \tag{20}$$

Now, assume that $\xi(x, y)$ be an isotropic random field [49, 56]. The property of isotropy requires that for any profile making an angle θ with x -axis, the following condition holds:

$$R(\rho \cos \theta, \rho \sin \theta) = R(\rho, 0). \tag{21}$$

From (16), (19), and (21), it follows that

$$R_{AC}(X, Y) = R_{CA}(X, -Y) = R_{AC}(-X, Y) = R_{AC}(\sqrt{X^2 + Y^2}, 0) = R_{\xi\xi}(\sqrt{X^2 + Y^2}). \tag{22}$$

Since autocorrelation function and PSD form a Fourier pair, cross-PSD is given by

$$S_{AC}(\Omega) = S_{CA}(\Omega) = (2\pi)^{-1} \int_{-\infty}^{\infty} R_{\xi\xi}(\sqrt{X^2 + Y^2})e^{-i\Omega X} dX. \tag{23}$$

Equations (19) and (23) are general results for spectral analysis under the hypothesis of isotropy. When using the definition of a normalized cross-PSD developed by Dodds and Robson [49], cross-PSD can also be written as

$$S_{AC}(\Omega) = S_{CA}(\Omega) = g(\Omega)S_{\xi\xi}(\Omega). \tag{24}$$

where $g(\Omega)$ is coherence function between direct-PSD and cross-PSD of two parallel wheel paths, which is always not

greater than 1 [57]. Heath [58] further presented a closed-form $g(\Omega)$

$$g(\Omega) = 1 - \frac{Y}{S_{\zeta\zeta}(\Omega)} \int_0^\infty S_{\zeta\zeta}(\sqrt{\Omega^2 + \zeta^2}) J_1(Y\zeta) d\zeta, \quad (25)$$

where $J_1(\cdot)$ is the first-order Bessel function and $\Omega \geq 0$.

2.2.2 The hypothesis of uncorrelation

Parkhilovskii [55] proposed the hypothesis of uncorrelation. It assumes that the two profiles of two parallel wheel paths, $\zeta(x, y_1)$ and $\zeta(x, y_2)$, can be derived from two uncorrelated random fields, that is

$$\zeta(x, y_1) = \zeta(x) + Y\gamma(x), \quad (26a)$$

$$\zeta(x, y_2) = \zeta(x) - Y\gamma(x). \quad (26b)$$

It then follows that

$$S_{AB}(\Omega) = S_{DC}(\Omega) = S_{\zeta\zeta}(\Omega) + Y^2 S_{\gamma\gamma}(\Omega), \quad (27a)$$

$$S_{AC}(\Omega) = S_{DB}(\Omega) = S_{\zeta\zeta}(\Omega) - Y^2 S_{\gamma\gamma}(\Omega). \quad (27b)$$

Thus, direct- and cross-PSD can be expressed in terms of direct PSDs of $\zeta(x)$ and $\gamma(x)$. Robson [59] has examined the physical and mathematical basis of Parkhilovskii model. He concluded that Parkhilovskii model can be made compatible with isotropic model for a profile-pair description of pavement (i.e., two parallel railway tracks), and may be used where isotropy assumption is not valid.

2.2.3 The Hypothesis of Shift

Sun and Su [60] proposed the hypothesis of shift to construct two-dimensional PSD using one-dimensional PSD. According to homogeneity in (19), autocorrelations of $\zeta(x, y_1)$ and $\zeta(x, y)$ equal to each other. Sun and Su [60] assumed $\zeta(x_1 + X, y_1 + Y) = \zeta(x_1 + X + s, y_1 + Y)$. In other words, the elevation of one wheel path is equal to the elevation of a parallel but shifted wheel path with a spatial lag s . With

$$\begin{aligned} R_{AC}(X, Y) &= E[\zeta(x_1, y_1)\zeta(x_1 + X, y_1 + Y)] \\ &= E[\zeta(x_1, y_1)\zeta(x_1 + X + s, y_1 + Y)] \\ &= R_{\zeta\zeta}(X + s), \end{aligned} \quad (28)$$

where spatial lag s is a parameter that can be estimated from field test of autocorrelation functions of parallel wheel path. Some properties about the spatial lag can be $s = 0$ as $Y = 0$ where $R_{AC}(X, 0) = R_{\zeta\zeta}(X)$ and $s \rightarrow \infty$ as $Y \rightarrow \infty$ where $R_{AC}(X, \infty) = 0$.

Under the hypothesis of shift, since PSD is the Fourier transform of correlation function, we have

$$S_{AC}(\Omega) = S_{CA}(\Omega) = (2\pi)^{-1} \int_{-\infty}^\infty R_{\zeta\zeta}(X + s) e^{-i\Omega X} dX. \quad (29)$$

Note that

$$R_{\zeta\zeta}(X + s) = \int_{-\infty}^\infty S_{\zeta\zeta}(K) e^{iK(X+s)} dK. \quad (30)$$

Replacing $R_{\zeta\zeta}(X + s)$ in (29) by (30) we obtain

$$\begin{aligned} S_{AC}(\Omega) &= S_{CA}(\Omega) \\ &= (2\pi)^{-1} \int_{-\infty}^\infty \int_{-\infty}^\infty S_{\zeta\zeta}(K) e^{iK(X+s)} e^{-i\Omega X} dX dK. \end{aligned} \quad (31)$$

Reversing the order of integration and using the convergence concept of a generalized function we have the inner integral

$$e^{iKs} \int_{-\infty}^\infty S_{\zeta\zeta}(K) e^{i(K-\Omega)X} dX = 2\pi\delta(K - \Omega) e^{iKs}. \quad (32)$$

Here the following integral is used [61]

$$\int_{-\infty}^\infty e^{iZX} dX = 2\pi\delta(Z). \quad (33)$$

Substituting (32) into (31) we get

$$S_{AC}(\Omega) = S_{CA}(\Omega) = S_{\zeta\zeta}(\Omega) e^{is\Omega}. \quad (34)$$

Here the property of Dirac delta function (Lighthill 1958)

$$\int_{-\infty}^\infty f(t)\delta(t - t_0) dt = f(t_0). \quad (35)$$

is used in the derivation of (34).

In summary, several used assumptions related to pavement surface are homogeneity, ergodicity and normal distribution. These have been supported by a number of measurements of pavement surface. However, there are still counterexamples demonstrating the existence of pavement surfaces that do not satisfy the homogeneous and ergodic properties [62]. In those situations, pavement surfaces are perceived by a vehicle as nonstationary stochastic processes [47, 63, 64]. It is worthwhile noting that nowadays with technology advancement, one can measure and obtain entire two-dimensional topology of pavement surface using remote sensing, line scanning laser, and synthetic aperture radar. For more accurate applications, it is no longer necessary to use hypothetical random field model of pavement surface.

3 Contact force on vehicle-pavement interface

Wheel loads in specifications of highway and airport pavement design are presently treated as a static load pressure with uniform distribution [65]

$$P(r) = P_0/\pi r_0^2 \text{ for } |r| \leq r_0, \quad (36)$$

where r_0 is the radius of circle distribution of wheel loads and P_0 represents the total loads applied. Such a simplification of actual vehicle/aircraft load in design can be adequate when the speed of travel is low and pavement surface is smooth. However, when the speed of travel is high and pavement surface is uneven due to deterioration, influence of dynamic load generated by vehicle–pavement interaction can become very significant. As a matter of fact, pavement damage is directly resulting from a long-term effect of dynamic traffic loading. Therefore, contact force on vehicle–pavement interface needs to be considered in pavement design to more closely reflect actual loading condition.

All pavement surfaces exhibit irregularities that cause vehicle vibration, which, in turn, results in moving stochastic contact forces on pavement [66]. At low speed of travel vehicle vibration is insignificant but at high speed of travel vehicle may vibrate significantly due to poor pavement surface conditions. It does not only reduce the ride quality but also generates additional damage to vehicle and pavement structures beyond static load.

The interaction between vehicles and pavements has been investigated extensively by the automobile industry for improving ride quality and reducing the mechanical fatigue of vehicle [5, 25, 50, 67–69]. Hedric [9], Abbo et al. [10], and Markow et al. [70] identified some critical factors that affect dynamic loads on pavement. These factors include vehicle and axle configuration, vehicle load, suspension characteristics (stiffness, damping), speed of travel, pavement roughness, faults, joint spacing and slab warping. From the perspective of pavement design and maintenance, however, little has been known about the effects of vehicle vibration on response, damage and performance of pavement structures [20, 54]. Although some efforts have been devoted to the measurement and prediction of dynamic wheel loads [4, 6, 11, 12, 71, 72], few of them provides a complete theoretical foundation for describing contact force induced by vehicle–pavement interaction. This can be a crucial element leading to a more precise dynamic analysis of pavement structures [54, 73, 74].

Of three approaches for studying vibration-generated contact forces, namely, analytic, experimental, and numerical simulation methods, only the last two have been used widely. Experimental method offers real results, it is however very costly and limited by safety requirements. Moreover, results from experimental method only suits in some degree for specific test conditions (e.g., vehicle and pavement types, speed of travel) [54]. In many circumstances, numerical simulation associated with a limited field tests serves as the most prevailing approach.

Numerical simulation has the advantage of capable of extrapolating experimental results over a range of test conditions where the experiment would be too dangerous

or too expensive. To study the contact forces between vehicle and pavement using numerical simulation, a vehicle must be simplified to a vehicle model so as to simulate the real operation conditions of the vehicle. Then, based on the vehicle model associated with measured or simulated pavement surface roughness, dynamic contact forces can be generated using a validated vehicle simulation program.

3.1 Pavement surface as a source of excitation to vehicle

As far as the vehicle vibration is concerned, pavement surface serves as a source of excitation when the vehicle travels along the road. As such, spatial fluctuation of pavement surface gets converted to temporal random excitation of vehicle suspension system. In this article, we assume that the speed of travel is constant. Different stochastic process of excitation can be resulting from different hypotheses on two-dimensional random field of pavement surface, which are present in this section.

3.1.1 General two-dimensional random field

Let $\mathbf{x} = (x, y)$ be the fixed coordinates in which the spatial random field is defined. Let $\mathbf{x}' = (x', y')$ be the moving coordinates connected with the moving vehicle and travel at the constant speed \mathbf{v} (vector quantity) with respect to the fixed coordinates \mathbf{x} . Denote $\mathbf{R}_\xi(\mathbf{x}_1, \mathbf{x}_2)$ the correlation function that describes the spatial random field $\xi(\mathbf{x})$. Denote $\mathbf{R}_\eta(\mathbf{x}'_1, \mathbf{x}'_2; t_1, t_2)$ the correlation function that describes the temporal random excitation $\eta(\mathbf{x}', t)$. Since

$$\eta(\mathbf{x}', t) = \xi(\mathbf{x}' + \mathbf{v}t), \tag{37}$$

we have

$$\mathbf{R}_\eta(\mathbf{x}'_1, \mathbf{x}'_2; t_1, t_2) = \mathbf{R}_\xi(\mathbf{x}'_1 + \mathbf{v}t_1, \mathbf{x}'_2 + \mathbf{v}t_2). \tag{38}$$

From the assumption mentioned above, $\xi(\mathbf{x})$ is a homogeneous random field. Accordingly, its correlation function $\mathbf{R}_\xi(\mathbf{x}_1, \mathbf{x}_2)$ becomes $\mathbf{R}_\xi(\mathbf{X})$ where $\mathbf{X} = \mathbf{x}_2 - \mathbf{x}_1$. Since vehicle velocity is a constant vector, the homogenous random field $\eta(\mathbf{x}', t)$ in spatial domain is converted to a stationary stochastic process in time domain. In other words, (38) can be replaced by

$$\mathbf{R}_\eta(\mathbf{X}', \tau) = \mathbf{R}_\xi(\mathbf{X}' + \mathbf{v}\tau), \tag{39}$$

where $\mathbf{X}' = \mathbf{x}'_2 - \mathbf{x}'_1$ and $\tau = t_2 - t_1$. Now we define $S_\xi(\boldsymbol{\Omega})$ as the spatial PSD of two-dimensional random field, i.e.,

$$\mathbf{S}_\xi(\boldsymbol{\Omega}) = (2\pi)^{-2} \int_{R^2} \mathbf{R}_\xi(\mathbf{X}) e^{-i\boldsymbol{\Omega}\mathbf{X}} d\mathbf{X}. \tag{40}$$

The PSD of random excitation $\eta(\mathbf{x}', t)$ can be expressed as

$$\mathbf{S}_\eta(\boldsymbol{\Omega}, \omega) = \mathbf{S}_\xi(\boldsymbol{\Omega})\delta(\omega - \boldsymbol{\Omega}\mathbf{v}). \tag{41}$$

Equation (41) can be proved as follows. Since

$$\mathbf{R}_\eta(\mathbf{X}', \tau) = \int_{-\infty}^{\infty} \int_{R^2} \mathbf{S}_\eta(\boldsymbol{\Omega}, \omega) e^{i(\boldsymbol{\Omega}\mathbf{X}' + \omega\tau)} d\boldsymbol{\Omega} d\omega. \tag{42}$$

Applying Eqs. (41) to (42) gives

$$\begin{aligned} \mathbf{R}_\eta(\mathbf{X}', \tau) &= \int_{R^2} [\mathbf{S}_\eta(\boldsymbol{\Omega}) e^{i\boldsymbol{\Omega}\mathbf{X}'} \int_{-\infty}^{\infty} \delta(\omega - \boldsymbol{\Omega}\mathbf{v}) e^{i\omega\tau} d\omega] d\boldsymbol{\Omega} \\ &= \mathbf{R}_\xi(\mathbf{X}' + \mathbf{v}\tau). \end{aligned} \tag{43}$$

$$S_{\eta_i\eta_j}(X_{ij}, \omega) = \begin{cases} \frac{1}{v} \left[\int_{-\infty}^{\infty} \mathbf{S}_\xi\left(\frac{\omega}{v}, K\right) dK \right] e^{i\omega X_{ij}/v} & \text{if } i \text{ and } j \text{ are located in the same side} \\ \frac{1}{v} \left[\int_{-\infty}^{\infty} \mathbf{S}_\xi\left(\frac{\omega}{v}, K\right) e^{iKY_0} dK \right] e^{i\omega X_{ij}/v} & \text{if } i \text{ and } j \text{ are located in the different side} \end{cases} \tag{50}$$

This is the same as Eq. (39). It is necessary to represent the PSD of random excitation $\eta(\mathbf{x}', t)$ in terms of angular frequency ω and spatial lag \mathbf{X}' , i.e.,

$$\mathbf{S}_\eta(\mathbf{X}', \omega) = \frac{1}{2\pi} \int_{-\infty}^{\infty} \mathbf{R}_\xi(\mathbf{X}' + \mathbf{v}\tau) e^{-i\omega\tau} d\tau. \tag{44}$$

If the direction of vehicle velocity vector is the same as that of the x -axis, then the following transformation applies:

$$X' + v\tau = X, Y' = Y \text{ and } v = |\mathbf{v}|. \tag{45}$$

Substituting (45) into (44), (9) is converted to

$$\mathbf{S}_\eta(\mathbf{X}', \omega) = \frac{1}{2\pi v} \int_{-\infty}^{\infty} \mathbf{R}_\xi(\mathbf{X}) e^{-i\omega X/v} dX e^{i\omega X'/v}, \tag{46}$$

where $\mathbf{X} = (X, Y)$ and $\mathbf{X}' = (X', Y')$. Corresponding to (40), spatial correlation function $\mathbf{R}_\xi(\mathbf{X})$ is the inverse Fourier transform of the spatial PSD $\mathbf{S}_\xi(\boldsymbol{\Omega})$, i.e.,

$$\mathbf{R}_\xi(\mathbf{X}) = \int_{R^2} \mathbf{S}_\xi(\boldsymbol{\Omega}) e^{i\boldsymbol{\Omega}\mathbf{X}} d\boldsymbol{\Omega}, \tag{47}$$

where $\boldsymbol{\Omega} = (\Omega, K)$. Combining Eqs. (47) and (46), we obtain

$$\mathbf{S}_\eta(\mathbf{X}', \omega) = \frac{1}{v} \left[\int_{-\infty}^{\infty} \mathbf{S}_\xi\left(\frac{\omega}{v}, K\right) e^{iKY} dK \right] e^{i\omega X'/v}. \tag{48}$$

In the derivation of (13), the following equation is used.

$$\int_{-\infty}^{\infty} e^{-iX(\frac{\omega}{v} - \Omega)} dX = 2\pi\delta\left(\frac{\omega}{v} - \Omega\right). \tag{49}$$

Equation (48) is a general result applicable to any form of two-dimensional random field. Under the restriction of the specified vehicle systems, we can represent (48) furthermore.

Figure 8 shows a plan view of a vehicle with N tires. We now consider the cross-PSD of between i th and j th tires. It is clear that if i th and j th tires are located in the same side of the vehicle, either in the left side or in the right side, then we should have $X' = X_{ij}$ and $Y = 0$. If i th tire is located in right side and j th tire is located in left side, or vice versa, then we should have $X' = X_{ij}$ and $Y = 0$.

Given Fig. 7 condition, (48) can be written in terms of spatial PSD roughness:

where $X_{ij} = x_j - x_i$ ($i, j = 1, 2, \dots, N$). As for direct-PSD excitation, we have $X_{ij} = 0$ ($i = j$) and $Y_0 = 0$. From Eq. (50) we get

$$S_{\eta_i\eta_i}(X_{ii}, \omega) = \frac{1}{v} \left[\int_{-\infty}^{\infty} \mathbf{S}_\xi\left(\frac{\omega}{v}, K\right) dK \right], \quad i = 1, 2, \dots, N. \tag{51}$$

Since the correlation function $\mathbf{R}_\xi(\mathbf{X})$ and PSD function $\mathbf{S}_\xi(\boldsymbol{\Omega})$ of the two-dimensional random field are both known from (40) and (47), there is no obstacle to compute the excitation PSD of (40) and (41).

3.1.2 Two-dimensional random field under hypothesis of isotropy

When pavement surface is treated as a two-dimensional random field under hypothesis of isotropy [56, 58], its two-dimensional PSD can be represented in terms of one-dimensional PSD. In other words, in light of (26) and the definition of two-dimensional PSD (40), the two-dimensional PSD can be constructed from the following Fourier transform:

$$\mathbf{S}_\xi(\boldsymbol{\Omega}) = (2\pi)^{-2} \int_{R^2} R_{\xi\xi}(\sqrt{X^2 + Y^2}) e^{-i(\Omega X + KY)} dX dY. \tag{52}$$

Notice that

$$\begin{aligned} &\int_{-\infty}^{\infty} \mathbf{S}_\xi(\boldsymbol{\Omega}) e^{iKY_0} dK \\ &= (2\pi)^{-2} \int_{-\infty}^{\infty} \int_{R^2} R_{\xi\xi}(\sqrt{X^2 + Y^2}) e^{-i(\Omega X + KY)} e^{iKY_0} dX dY dK \\ &= (2\pi)^{-1} \int_{-\infty}^{\infty} R_{\xi\xi}(\sqrt{X^2 + Y_0^2}) e^{-i\Omega X} dX \end{aligned} \tag{53}$$

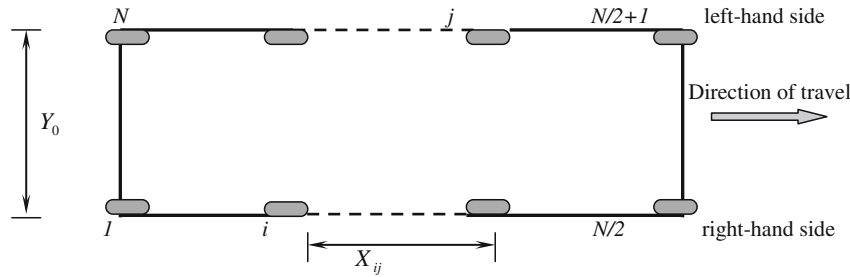


Fig. 8 A plane view of an N-tire vehicle model

Here, the general integration [61]

$$\int_{-\infty}^{\infty} e^{-iK(Y-Y_0)} dK = 2\pi\delta(Y - Y_0) \tag{54}$$

and (30b), respectively. Without any difficulty, it is straightforward to see that (40) and (41) can be further written as

$$S_{\eta_i\eta_j}(X_{ij}, \omega) = \begin{cases} \frac{1}{v} [S_{\zeta\zeta}(\frac{\omega}{v}) + Y_0^2 S_{\gamma\gamma}(\frac{\omega}{v})] e^{i\omega X_{ij}/v} & \text{if } i \text{ and } j \text{ are located in the same side} \\ \frac{1}{v} [S_{\zeta\zeta}(\frac{\omega}{v}) - Y_0^2 S_{\gamma\gamma}(\frac{\omega}{v})] e^{i\omega X_{ij}/v} & \text{if } i \text{ and } j \text{ are located in the different side} \end{cases} \tag{58}$$

and the property of Dirac delta function [75]

$$\int_{-\infty}^{\infty} f(x)\delta(x - x_0)dx = f(x_0) \tag{55}$$

are used in the derivation of Eq. (53).

Comparing (53) with (27), it is clear that the left side of (53) is just the PSD given by $S_{AC}(\Omega)$. Since it has been proved that $S_{AC}(\Omega) = g(\Omega)S_{\zeta\zeta}(\Omega)$ where $g(\Omega)$ is an ordinary coherence function and $S_{\zeta\zeta}(\Omega)$ is one-dimensional PSD roughness. Hence, (40) and (41) can be further expressed as

$$S_{\eta_i\eta_j}(X_{ij}, \omega) = \begin{cases} \frac{1}{v} S_{\zeta\zeta}(\frac{\omega}{v}) e^{i\omega X_{ij}/v} & \text{if } i \text{ and } j \text{ are located in the same side} \\ \frac{1}{v} g(\frac{\omega}{v}) S_{\zeta\zeta}(\frac{\omega}{v}) e^{i\omega X_{ij}/v} & \text{if } i \text{ and } j \text{ are located in the different side} \end{cases} \tag{56}$$

and

$$S_{\eta_i\eta_i}(X_{ii}, \omega) = \frac{1}{v} S_{\zeta\zeta}(\frac{\omega}{v}), \quad i = 1, 2, \dots, N. \tag{57}$$

3.1.3 Two-dimensional random field under hypothesis of uncorrelation

When pavement surface is treated as a two-dimensional random field under hypothesis of uncorrelation [55], the integration of the left side of (53) becomes either $S_{AB}(\Omega)$ if i and j are located on the same side of the vehicle, or $S_{AC}(\Omega)$ if i and j are located on the different side of the vehicle, which are further given by (30a)

and

$$S_{\eta_i\eta_i}(X_{ii}, \omega) = \begin{cases} \frac{1}{v} [S_{\zeta\zeta}(\frac{\omega}{v}) + Y_0^2 S_{\gamma\gamma}(\frac{\omega}{v})] & \text{if } i \text{ is located in the right side } i = 1, 2, \dots, N. \\ \frac{1}{v} [S_{\zeta\zeta}(\frac{\omega}{v}) - Y_0^2 S_{\gamma\gamma}(\frac{\omega}{v})] & \text{if } i \text{ is located in the left side} \end{cases} \tag{59}$$

3.1.4 Two-dimensional random field under hypothesis of shift

When pavement surface is constructed from a two-dimensional random field under hypothesis of shift, (40) and (41) can be written as

$$S_{\eta_i\eta_j}(X_{ij}, \omega) = \begin{cases} \frac{1}{v} S_{\zeta\zeta}(\frac{\omega}{v}) e^{i\omega X_{ij}/v} & \text{if } i \text{ and } j \text{ are located in the same side} \\ \frac{1}{v} S_{\zeta\zeta}(\frac{\omega}{v}) e^{i\omega(X_{ij}+s)/v} & \text{if } i \text{ and } j \text{ are located in the different side} \end{cases} \tag{60a}$$

and

$$S_{\eta_i\eta_i}(X_{ii}, \omega) = \begin{cases} \frac{1}{v} S_{\zeta\zeta}(\frac{\omega}{v}) & \text{if } i \text{ is located in the right side } i = 1, 2, \dots, N. \\ \frac{1}{v} S_{\zeta\zeta}(\frac{\omega}{v}) e^{i\omega s/v} & \text{if } i \text{ is located in the left side} \end{cases} \tag{60b}$$

3.2 Vehicle models

Here, we consider vehicle models for simulating dynamic contact forces. Three kinds of vehicle models are commonly used nowadays, i.e., quarter-vehicle, half-vehicle,

and full-vehicle models. Making a reasonable choice between a complex vehicle model and a simple vehicle model relies on the nature of the problem. The advantage of the complex vehicle model is that it can accurately predict the acceleration response at different locations of the vehicle. The complex vehicle model is thus suitable for studying influences of vehicle vibrations on human body and the fatigue life of vehicles caused by vehicle vibrations. However, the complex vehicle model is highly sophisticated and requires detailed input and long execution times even for simple problems. Because vehicle sizes and loads vary greatly, it is more difficult to select representative parameter values for the complex vehicle model than for the simple vehicle model, which increases the difficulty to compare computer simulation results conducted by different research groups. This should be always kept in mind.

In Sect. 3.1, pavement surface is converted into a stationary stochastic process as input to excite vehicle vibration when the vehicle travels at a constant speed. To proceed further, we also assume that vehicle's suspension system is linear, under which the equations of motion of vehicle suspension systems for small oscillations can be derived using the Lagrange equations.

Let \mathbf{Y} be a set of M independent generalized coordinates (e.g., the absolute displacement of components of vehicle systems) that completely specify the configuration of the system measured from the equilibrium position. Then, the kinetic energy T , potential energy U , and dissipative energy D , can be expressed as

$$T = \frac{1}{2} \dot{\mathbf{Y}}^T \mathbf{M}^{abs} \dot{\mathbf{Y}}, \tag{61a}$$

$$U = \frac{1}{2} \dot{\mathbf{Y}}^T \mathbf{K}^{abs} \dot{\mathbf{Y}}, \tag{61b}$$

$$D = \frac{1}{2} \dot{\mathbf{Y}}^T \mathbf{C}^{abs} \dot{\mathbf{Y}}, \tag{61c}$$

where \mathbf{M}^{abs} , \mathbf{K}^{abs} and \mathbf{C}^{abs} are mass, stiffness, and viscous damping matrices with respect to absolute displacement vector $\mathbf{Y} = \{Y_1, Y_2, \dots, Y_M\}^T$, respectively. The Lagrange equations of motion are

$$\frac{d}{dt} \left(\frac{\partial T}{\partial \dot{\mathbf{Y}}_j} \right) + \frac{\partial D}{\partial \dot{\mathbf{Y}}_j} + \frac{\partial U}{\partial \mathbf{Y}_j} = 0 \quad v = |\mathbf{v}| \quad j = 1, 2, \dots, M. \tag{62}$$

Under the assumption that all components of the vehicle system be linear, (61) and (62) yield a set of simultaneous second-order differential equations with constant coefficients:

$$\begin{aligned} & \mathbf{M}^{abs} \left\{ \ddot{\mathbf{Y}} \right\} + \mathbf{C}^{abs} \left\{ \dot{\mathbf{Y}} \right\} + \mathbf{K}^{abs} \left\{ \mathbf{Y} \right\} \\ & = \mathbf{C}_f^{abs} \left\{ \dot{\eta} \right\} + \mathbf{K}_f^{abs} \left\{ \eta \right\} = \left\{ \mathbf{F}^{abs}(t) \right\}, \end{aligned} \tag{63}$$

where $\boldsymbol{\eta}$ and $\dot{\eta}$ are, respectively, the pavement surface elevation vector and its derivative process. Clearly, here we assume that the contact between tires and pavement surface is in the form of point distribution.

Without loss of generality, let components of the vehicle system directly contacting with ground in the moving coordinates \mathbf{x}' be numbered from 1 to N (see Fig. 7), where N represents the total number of tires. Let

$$\begin{cases} Z_i = Y_i - \eta_i & \text{for } i = 1, 2, \dots, N \\ Z_i = Y_i & \text{for } i = N + 1, N + 2, \dots, M \end{cases} \tag{64}$$

Equation (63) can be rewrote as

$$\mathbf{M}\{\mathbf{Z}\} + \mathbf{C}\{\mathbf{Z}\} + \mathbf{K}\{\mathbf{Z}\} = \mathbf{C}_f\{\dot{\eta}\} + \mathbf{K}_f\{\eta\} = \{\mathbf{F}(t)\}, \tag{65}$$

where \mathbf{M} , \mathbf{K} and \mathbf{C} are mass, stiffness, and viscous damping matrices with respect to relative displacement $\mathbf{Z} = \{Z_1, Z_2, \dots, Z_M\}^T$, respectively. Since the total number of degree of freedom is assumed to be M , and η is N -dimensional temporal excitation vector representing pavement surface-induced displacements in coordinates \mathbf{x}' , \mathbf{M} , \mathbf{K} , and \mathbf{C} are M by M matrices, \mathbf{C}_f , and \mathbf{K}_f are M by N matrices, and force vector $\mathbf{F}(t)$ is an M by 1 matrix. Equations (63) and (64) represent a linear mathematical model of vehicle systems. Taking Fourier transform to both sides of Eq. (65), we have

$$\begin{aligned} & [-\omega^2 \mathbf{M} + i\omega \mathbf{C} + \mathbf{K}]_{M \times M} \{\tilde{\mathbf{Z}}\}_{M \times 1} \\ & = [i\omega \mathbf{C}_f + \mathbf{K}_f]_{M \times N} \{\tilde{\eta}\}_{N \times 1}, \end{aligned} \tag{66}$$

in which $\tilde{\mathbf{Z}}$ and $\tilde{\eta}$ are, respectively, the Fourier transform of \mathbf{Z} and η , i.e.,

$$\tilde{\mathbf{Z}}(\omega) = \frac{1}{2\pi} \int_{-\infty}^{\infty} \mathbf{Z}(t) e^{-i\omega t} dt, \tag{67a}$$

$$\tilde{\eta}(\omega) = \frac{1}{2\pi} \int_{-\infty}^{\infty} \eta(t) e^{-i\omega t} dt. \tag{67b}$$

Multiplying the inverse matrix of $[-\omega^2 \mathbf{M} + i\omega \mathbf{C} + \mathbf{K}]$, it is straightforward to see

$$\{\tilde{\mathbf{Z}}\} = [-\omega^2 \mathbf{M} + i\omega \mathbf{C} + \mathbf{K}]^{-1} [i\omega \mathbf{C}_f + \mathbf{K}_f] \{\tilde{\eta}\}. \tag{68}$$

The primary aim of establishing vehicle models is to find the scalar response of $\mathbf{Z}(t)$ as well as $\tilde{\mathbf{Z}}(\omega)$. This can be accomplished by using stochastic process theory of linear systems. The dynamic characteristics of the vehicle at angular frequency ω are defined by $M \times N$ frequency response function (FRF) matrix, $H(\omega)$, of the vehicle system, where $H(\omega) = [H(\omega)_{ij}]$, $i = 1, 2, \dots, M$ for the M outputs and $j = 1, 2, \dots, N$ for the N inputs of pavement excitation to tires. These functions are defined as follows. If a vertical displacement $\eta_j(t) = e^{i\omega t}$ is applied to the vehicle at j th tire, with all the other inputs being zero, then

the response of the vehicle is given by $Z(t)_{ij} = H(\omega)_{ij}e^{i\omega t}$. Based on Eq. (68), it is straightforward to see that FRF matrix can be given by

$$\mathbf{H}(\omega) = [-\omega^2\mathbf{M} + i\omega\mathbf{C} + \mathbf{K}]_{M \times M}^{-1} [i\omega\mathbf{C}_f + \mathbf{K}_f]_{M \times N}. \quad (69)$$

Let

$$\mathbf{A} = \mathbf{AR} + i\mathbf{AI} = [-\omega^2\mathbf{M} + i\omega\mathbf{C} + \mathbf{K}]^{-1} \quad (70a)$$

and

$$\mathbf{Q} = \mathbf{QR} + i\mathbf{QI} = [i\omega\mathbf{C}_f + \mathbf{K}_f], \quad (70b)$$

where \mathbf{AR} and \mathbf{AI} , respectively, represent real and imaginary parts of matrix \mathbf{A} , \mathbf{QR} and \mathbf{QI} , respectively, represent real and imaginary parts of matrix \mathbf{Q} . It is convenient to express FRF matrix in terms of real part \mathbf{HR} and imaginary part \mathbf{HI}

$$\mathbf{H}(\omega) = \mathbf{HR} + i\mathbf{HI}, \quad (71)$$

where

$$\mathbf{HR} = \mathbf{AR} \cdot \mathbf{QR} - \mathbf{AI} \cdot \mathbf{QI},$$

$$\mathbf{HI} = \mathbf{AI} \cdot \mathbf{QR} + \mathbf{AR} \cdot \mathbf{QI}.$$

From the stochastic process theory, PSD response of a linear system and PSD excitation satisfy the following relationship [76]:

$$\mathbf{S}_Z(X_{ij}, \omega) = \mathbf{H}^*(\omega) \mathbf{S}_\eta(X_{ij}, \omega) \mathbf{H}^T(\omega) \quad (72a)$$

$$M \times M \quad M \times N \quad N \times N \quad N \times M.$$

or equivalently,

$$S_{Z_i Z_j}(X_{ij}, \omega) = \sum_{l=1}^N \sum_{k=1}^N H_{ik}^*(\omega) H_{jl}(\omega) S_{\eta_k \eta_l}(X_{kl}, \omega), \quad (72b)$$

where $\mathbf{S}_Z(X_{ij}, \omega) = [S_{Z_i Z_j}(X_{ij}, \omega)]_{M \times M}$, $\mathbf{S}_\eta(X_{ij}, \omega) = [S_{\eta_i \eta_j}(X_{ij}, \omega)]_{N \times N}$, $\mathbf{H}^*(\omega)$ and $\mathbf{H}^T(\omega)$ are, respectively, the conjugate matrix and the transposed matrix of FRF matrix $\mathbf{H}(\omega)$. It may be noticed that $\mathbf{H}^*(\omega)$ and $\mathbf{H}^T(\omega)$ can be, respectively, expressed in the form of real and imaginary parts by means of Eqs. (72a) and (72b)

$$\mathbf{H}^*(\omega) = \mathbf{HR} - i\mathbf{HI}, \quad (73a)$$

$$\mathbf{H}^T(\omega) = \mathbf{HR}^T + i\mathbf{HI}^T. \quad (73b)$$

Similarly, we may write $\mathbf{S}_Z(X_{ij}, \omega)$ as

$$\mathbf{S}_Z(X_{ij}, \omega) = \mathbf{SR}_Z(X_{ij}, \omega) + i\mathbf{SI}_Z(X_{ij}, \omega) \quad (74)$$

in which $\mathbf{SR}_Z(X_{ij}, \omega)$ and $\mathbf{SI}_Z(X_{ij}, \omega)$ are, respectively, the real and imaginary parts of response spectral density $\mathbf{S}_Z(\omega)$. If the pavement excitation spectral density $\mathbf{S}_\eta(\omega)$ is a real spectrum matrix, then by expanding (72b) using (73a) and (73b), we have

$$\mathbf{SR}_Z(X_{ij}, \omega) = \mathbf{HR} \cdot \mathbf{S}_\eta(X_{ij}, \omega) \cdot \mathbf{HR}^T + \mathbf{HI} \cdot \mathbf{S}_\eta(X_{ij}, \omega) \cdot \mathbf{HI}^T. \quad (75a)$$

and

$$\mathbf{SI}_Z(X_{ij}, \omega) = \mathbf{HR} \cdot \mathbf{S}_\eta(X_{ij}, \omega) \cdot \mathbf{HI}^T - \mathbf{HI} \cdot \mathbf{S}_\eta(X_{ij}, \omega) \cdot \mathbf{HR}^T. \quad (75b)$$

If the pavement excitation spectral density $\mathbf{S}_\eta(\omega)$ is a complex spectrum matrix, say

$$\mathbf{S}_\eta(X_{ij}, \omega) = \mathbf{SR}_\eta(X_{ij}, \omega) + i\mathbf{SI}_\eta(X_{ij}, \omega) \quad (76)$$

then by expanding Eqs. (72b) using (73a), (73b), and (76), we have

$$\mathbf{SR}_Z(X_{ij}, \omega) = [\mathbf{HR} \cdot \mathbf{SR}_\eta(X_{ij}, \omega) + \mathbf{HI} \cdot \mathbf{SI}_\eta(X_{ij}, \omega)] \cdot \mathbf{HR}^T, \\ - [\mathbf{HR} \cdot \mathbf{SI}_\eta(X_{ij}, \omega) - \mathbf{HI} \cdot \mathbf{SR}_\eta(X_{ij}, \omega)] \cdot \mathbf{HI}^T, \quad (77a)$$

and

$$\mathbf{SI}_Z(X_{ij}, \omega) = [\mathbf{HR} \cdot \mathbf{SI}_\eta(X_{ij}, \omega) - \mathbf{HI} \cdot \mathbf{SR}_\eta(X_{ij}, \omega)] \cdot \mathbf{HR}^T \\ + [\mathbf{HR} \cdot \mathbf{SR}_\eta(X_{ij}, \omega) - \mathbf{HI} \cdot \mathbf{SI}_\eta(X_{ij}, \omega)] \cdot \mathbf{HI}^T. \quad (77b)$$

3.3 Dynamic load

3.3.1 Time-domain analysis

Figure 9 shows a sketch of the i th tire contacted with rough pavement surface. From Newton's second law of motion it is direct to know that the contact force between i th tire and pavement, $P_i(t)$, can be given by

$$P_i(t) = k_i Z_i(t) + c_i \dot{Z}_i(t), \quad i = 1, 2, \dots, N, \quad (78)$$

where k_i and c_i , respectively, the i th tire spring stiffness and viscous damping, both being constant. According to stochastic process theory, if the input of a linear time-invariable system is a stationary random process, then the output of the system is also a stationary random process [76]. As was noted, since temporal random excitation of pavement surface Gaussian ergodic random process with zero mean, the response $Z_i(t)$ and its derivative process $\dot{Z}_i(t)$ are both zero mean Gaussian stationary stochastic processes. Taking expectation to both sides of (78), we get the mean function of dynamic contact forces, m_P

$$m_{P_i}(t) = E[P_i(t)] = k_i E[Z_i(t)] + c_i E[\dot{Z}_i(t)] = 0. \quad (79)$$

It should be pointed out that the mean function $m_P(t)$ here, not containing the static load of vehicle, only represents the statistical average of dynamic effect. If the static load is considered, then the complete mean function of dynamic contact forces, \bar{P}_i , is given by

$$\bar{P}_i = m_{P_i}(t) + P_{0i} = m_i g, \tag{80}$$

where g is the acceleration due to gravity, P_{0i} and m_i are, respectively, the effective weight and effective mass distributed by the vehicle on i th tire. Without special statements, the derivation of formulation in the context is based on (79).

It is of interest to know the correlation function of dynamic contact forces between vehicle and pavement because this information is critical for analyzing the dynamic response of pavement structure under vehicle loads. According to the definition of correlation function and using Eq. (78), we have

$$\begin{aligned} R_{P_i P_j}(X_{ij}, \tau) &= E[P_i(t)P_j(t + \tau)] \\ &= k_i k_j R_{Z_i Z_j}(X_{ij}, \tau) + c_i c_j R_{\dot{Z}_i \dot{Z}_j}(X_{ij}, \tau) \\ &\quad + k_i c_j R_{Z_i \dot{Z}_j}(X_{ij}, \tau) + c_i k_j R_{\dot{Z}_i Z_j}(X_{ij}, \tau). \end{aligned} \tag{81}$$

It is known from stochastic differential principles that there exists exchangeability between expectation and square differential [31]. In other words, if a random process $Z(t)$ is differentiable for any order, it is proved that

$$\frac{\partial^{n+m}}{\partial t^n \partial s^m} R_{ZZ}(t, s) = R_{Z^{(n)} Z^{(m)}}(t, s), \tag{82}$$

where $Z^{(n)} = d^n Z(t)/dt^n$. In addition, if $Z(t)$ is a stationary process, then (73a) becomes

$$(-1)^n \frac{\partial^{n+m}}{\partial \tau^{n+m}} R_{ZZ}(\tau) = R_{Z^{(n)} Z^{(m)}}(\tau). \tag{83}$$

Applying Eq. (83) into Eq. (81) gives

$$\begin{aligned} R_{P_i P_j}(X_{ij}, \tau) &= k_i k_j R_{Z_i Z_j}(X_{ij}, \tau) - c_i c_j \frac{\partial^2}{\partial \tau^2} R_{Z_i Z_j}(X_{ij}, \tau) \\ &\quad + k_i c_j \frac{\partial}{\partial \tau} R_{Z_i Z_j}(X_{ij}, \tau) - c_i k_j \frac{\partial}{\partial \tau} R_{Z_i Z_j}(X_{ij}, \tau). \end{aligned} \tag{84}$$

It is clearly seen that autocorrelation function is obtained as $i = j$

$$R_{P_i P_i}(X_{ij}, \tau) = k_i^2 R_{Z_i Z_i}(X_{ij}, \tau) - c_i^2 \frac{\partial^2}{\partial \tau^2} R_{Z_i Z_i}(X_{ij}, \tau), \tag{85}$$

and crosscorrelation function is obtained as $i \neq j$.

3.3.2 Frequency-domain analysis

Having obtained correlation function, it is not difficult to represent the power spectral density (PSD), which is defined as the Fourier transform of correlation function. From Eq. (81) we have

$$\begin{aligned} S_{P_i P_j}(X_{ij}, \omega) &= k_i k_j S_{Z_i Z_j}(X_{ij}, \omega) + c_i c_j S_{\dot{Z}_i \dot{Z}_j}(X_{ij}, \omega) \\ &\quad + k_i c_j S_{Z_i \dot{Z}_j}(X_{ij}, \omega) + c_i k_j S_{\dot{Z}_i Z_j}(X_{ij}, \omega), \end{aligned} \tag{86}$$

where

$$S_{P_i P_j}(X_{ij}, \omega) = \frac{1}{2\pi} \int_{-\infty}^{\infty} R_{P_i P_j}(X_{ij}, \tau) e^{-i\omega\tau} d\tau, \tag{86a}$$

$$S_{Z_i Z_j}(X_{ij}, \omega) = \frac{1}{2\pi} \int_{-\infty}^{\infty} R_{Z_i Z_j}(X_{ij}, \tau) e^{-i\omega\tau} d\tau, \tag{86b}$$

$$S_{\dot{Z}_i \dot{Z}_j}(X_{ij}, \omega) = \frac{1}{2\pi} \int_{-\infty}^{\infty} R_{\dot{Z}_i \dot{Z}_j}(X_{ij}, \tau) e^{-i\omega\tau} d\tau, \tag{86c}$$

$$S_{Z_i \dot{Z}_j}(X_{ij}, \omega) = \frac{1}{2\pi} \int_{-\infty}^{\infty} R_{Z_i \dot{Z}_j}(X_{ij}, \tau) e^{-i\omega\tau} d\tau, \tag{86d}$$

$$S_{\dot{Z}_i Z_j}(X_{ij}, \omega) = \frac{1}{2\pi} \int_{-\infty}^{\infty} R_{\dot{Z}_i Z_j}(X_{ij}, \tau) e^{-i\omega\tau} d\tau. \tag{86e}$$

Correlation function $R_{P_i P_j}(\tau)$ is the Fourier inverse transform of PSD function $S_{Z_i Z_j}(\omega)$:

$$R_{Z_i Z_j}(X_{ij}, \omega) = \int_{-\infty}^{\infty} S_{Z_i Z_j}(X_{ij}, \tau) e^{i\omega\tau} d\omega. \tag{87}$$

Taking derivative to both sides of Eq. (87) gives [31, 182]

$$\frac{d^n}{d\tau^n} R_{Z_i Z_j}(X_{ij}, \omega) = i^n \int_{-\infty}^{\infty} \omega^n S_{Z_i Z_j}(X_{ij}, \tau) e^{i\omega\tau} d\omega. \tag{88}$$

By combining Eqs. (83) and (88), we find that

$$S_{\dot{Z}_i \dot{Z}_j}(X_{ij}, \omega) = \omega^2 S_{Z_i Z_j}(X_{ij}, \omega), \tag{88a}$$

$$S_{Z_i \dot{Z}_j}(X_{ij}, \omega) = i\omega S_{Z_i Z_j}(X_{ij}, \omega), \tag{88b}$$

$$S_{\dot{Z}_i Z_j}(X_{ij}, \omega) = -i\omega S_{Z_i Z_j}(X_{ij}, \omega). \tag{88c}$$

Substituting (88) into (84), we eventually get the PSD forces in terms of PSD of relative displacement response:

$$S_{P_i P_j}(X_{ij}, \omega) = [k_i k_j + c_i c_j \omega^2 + i\omega(k_i c_j - c_i k_j)] S_{Z_i Z_j}(X_{ij}, \omega). \tag{89}$$

Equation (89) applies to both direct-spectrum and cross-spectrum. In addition, as far as direct-spectrum is concerned, we can rewrite PSD forces in more concise form:

$$S_{P_i P_i}(\omega) = (k_i^2 + c_i^2 \omega^2) S_{Z_i Z_i}(\omega). \tag{90}$$

Standard deviation of contact forces can be expressed in terms of PSD forces. Applying Eq. (90) to the definition of standard deviation directly shows that

$$\sigma_{P_i}^2 = \int_{-\infty}^{\infty} S_{P_i P_i}(\omega) d\omega = \int_{-\infty}^{\infty} (k_i^2 + c_i^2 \omega^2) S_{Z_i Z_i}(\omega) d\omega. \tag{91}$$

Furthermore, if the standard deviations of displace response and velocity response, σ_{Z_i} and $\sigma_{\dot{Z}_i}$, are deployed, Eq. (91) can be rewritten as

$$\sigma_{P_i}^2 = k_i^2 \sigma_{Z_i}^2 + c_i^2 \sigma_{\dot{Z}_i}^2, \tag{92}$$

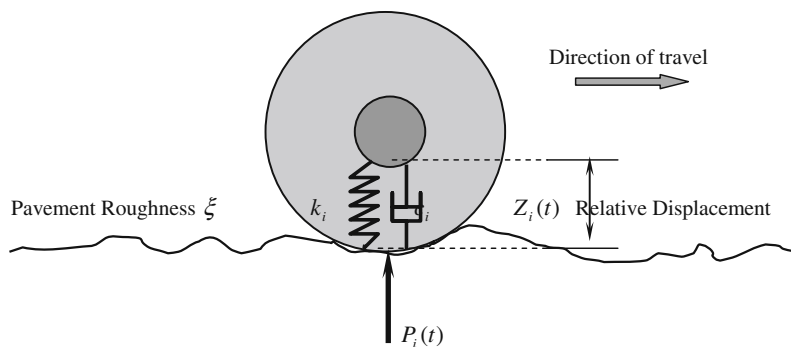


Fig. 9 A sketch of the *i*th tire on rough pavement surface

in which

$$\sigma_{Z_i}^2 = \int_{-\infty}^{\infty} S_{Z_i Z_i}(\omega) d\omega \text{ and } \sigma_{\dot{Z}_i}^2 = \int_{-\infty}^{\infty} \omega^2 S_{Z_i Z_i}(\omega) d\omega. \tag{93}$$

3.3.3 A Case Study of Walking-Beam Suspension System

As a case study, a walking-beam suspension system is shown in Fig. 10. Governing equations of this vehicle’s suspension system are also given by (65) in matrix form, where parameters and their values related to this walking-beam system are listed in Table 2 with $m_1 = 1,100$ kg, $m_2 = 3,900$ kg, $I = 465$ kgm², $s = 1.30$ m, $a_1 = a_2 = 0.5$, $k_1 = k_2 = 1.75$ (MN/s), $k_3 = 1.0$ (MN/s), $c_3 = 15.0$ (kNs/m), and $c_1 = c_2 = 2.0$ (kNs/m).

$$\mathbf{M} = \begin{bmatrix} 0 & 0 & m_2 \\ m_1 a_2 & m_1 a_1 & 0 \\ -I/b & I/b & 0 \end{bmatrix},$$

$$\mathbf{C} = \begin{bmatrix} -c_3 a_2 & -c_3 a_1 & c_3 \\ c_1 + c_3 a_2 & c_2 + c_3 a_1 & -c_3 \\ c_1 a_2 b & -c_2 a_1 b & 0 \end{bmatrix},$$

$$\mathbf{K} = \begin{bmatrix} -k_3 a_2 & -k_3 a_1 & k_3 \\ k_1 + k_3 a_2 & k_2 + k_3 a_1 & -k_3 \\ k_1 a_2 b & -k_2 a_1 b & 0 \end{bmatrix},$$

$$\{\mathbf{F}(t)\} = \begin{bmatrix} 0 & c_3 a_2 & k_3 a_2 & 0 & c_3 a_1 & k_3 a_1 \\ -m_1 a_2 & -c_3 a_2 & -k_3 a_2 & -m_1 a_1 & -c_3 a_1 & -k_3 a_1 \\ I/b & 0 & 0 & -I/b & 0 & 0 \end{bmatrix} \times \begin{Bmatrix} \dot{\eta}_1 \\ \dot{\eta}_1 \\ \eta_1 \\ \ddot{\eta}_2 \\ \dot{\eta}_2 \\ \eta_2 \end{Bmatrix}.$$

A two-dimensional isotropic random field is used for numerical simulation. The one-dimensional PSD roughness proposed by the International Organization for Standardization (ISO) in the power form [49, 52]

$$S_{\xi\xi}(\Omega) = S_0 \Omega^{-\gamma}, \tag{94}$$

with parameters $S_0 = 3.37 \times 10^{-6}$ m³/cycle and $\gamma = 2.0$ is adopted for numerical computation. Figure 11 shows the PSD contact force of the right tire at the speed of 20 m/s.

In aforementioned study, the contact area between the tire and the pavement surface is assumed as a point contact. There is no difficulty to extend this point contact to a distributed contact by considering the footprint as a weighted integration of contacting points [77–79]. It should be noted that the effect of nonlinearity in vehicle suspension and variable speed of travel (e.g., acceleration, deceleration, etc.), and inhomogeneity in pavement surface on contact force between vehicle and pavement have not been addressed here, which have been considered in various studies [80].

4 Pavement response under moving stochastic loads

4.1 Background

A large class of time-dependent sources such as vehicle, submarines, aircraft, and explosion-induced waves belongs to moving sources. The study of response of media (pavement, runway, rail-track, bridge, air, and sea) to moving sources is named moving source problem (MSP), which is of particular interest to structural design, noise assessment, target detection, etc. [81]. A number of studies have been addressed to MSP in various fields of physics. For instance, the response of an ice plate of finite thickness caused by moving loads was discussed by Strathdee et al. [82]. Wells and Han [83] analyzed the noise generated by a moving source in a moving medium. As for the aspect of

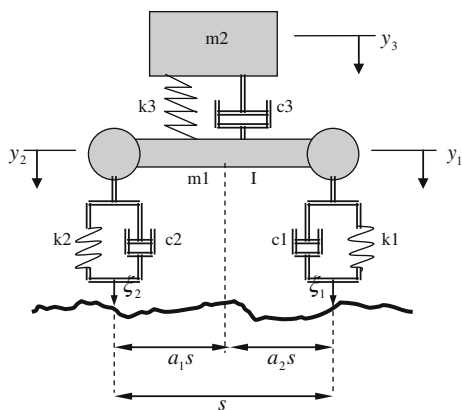


Fig. 10 A walking-beam suspension system

Table 2 Parameters used in the case study of walking-beam suspension system

Parameter	Description
m_1	Unsprung mass
m_2	Sprung mass
I	Moment inertia of unsprung mass
k_1	Spring stiffness of right side tire
k_2	Spring stiffness of left side tire
k_3	Spring stiffness of suspension
c_1	Damping of right side tire
c_2	Damping of left side tire
c_3	Damping of suspension
s	Effective width of the vehicle
y	Absolute vertical displacement of center of unsprung mass
y_1	Absolute vertical displacement of right side of unsprung mass
y_2	Absolute vertical displacement of left side of unsprung mass
y_3	Absolute vertical displacement of sprung mass
ξ_1	Absolute height of pavement profile along right wheel path
ξ_{2m}	Absolute height of pavement profile along left wheel path

elastodynamics, even more investigations are being done [84–94]. One may refer to Sun [95] for detailed review of MSP.

Methods for solving MSP primarily include integral transformation, characteristic curve, and modal analysis [96–100]. A common characteristic of previous studies is to utilize Galilean transform. The advantage of using Galilean transform is that the governing field equations, usually partial differential equations, can be reconstructed in a moving coordination so that the effect of source velocity may be reflected in parametric ordinary differential equations. However, since Galilean transform requires

that the source is steadily moving, the methods based on Galilean transform only apply to the steady-state solution. As for transient solution, a feasible way is to directly apply high-order integral transformation to the field equations. Since velocity parameter is included in boundary or initial condition, there is intractable obstacle when integrating the field equations. This can be the reason why most of the MSPs are solved only for steady-state solution.

As far as pavement response is concerned, some pioneers have dedicated their research to the subject of effects of moving loads on pavement structure. To perform the dynamic analysis of pavement structures, one of the indispensable considerations is the dynamic traffic loading, which is the excitation source of pavement structures. Since pavement loads are caused by vehicle vibration, it is necessary to include the vehicle in the investigations of pavement loads. Employing MIT heavy truck simulation program Hedric and his associates, Abbo and Markow [9–11], examined the influence of joint spacing, step faulting, vehicle suspension characteristics, and vehicle velocity on pavement damage as defined by fatigue cracking in concrete slab. The response of pavement under their consideration is achieved using PMARP, a static finite element program for pavement analysis developed by the Purdue. The conclusions obtain provide a valuable approximation of pavement response. While PMARP is a static finite element program, the properties of inertia and damping of the pavement structure were not included in consideration.

An advanced pavement model called MOVE program was developed by Chen [101] and Monismith et al. [73] at UC-Berkeley. This model can take the motion of load into account by means of finite element methods and is an important dedication to pavement structural analysis. The vehicle load is assumed to be an infinite line load to simplify the analysis from a three-dimensional problem to a two-dimensional problem. In addition, the model is based on the deterministic elastodynamics; therefore, neither pavement surface roughness nor vehicle suspension can be considered in the presented framework.

Since dynamic effects have been increasingly important in the prediction of pavement response, damage, and performance [14, 16, 18], it has become necessary to develop better mathematical models to account the effects of motion and fluctuation of contact forces caused by various types of vehicle suspensions [73]. The author has carried out a number of studies on deterministic and stochastic MSPs over the last two decades by providing a general approach that can include surface roughness and vehicle suspensions in the response of continuum media [54, 74].

The complexity in MSP is the variable load position, which not only makes the representation of the field

equation in time-invariant fixed coordinates difficult but also increases the difficulty of integration due to the appearance of speed parameter. In most of the previous MSP studies, some simple cases with deterministic conditions, for example, a constant load with uniform speed, are considered. However, the research on dynamic response of

continuum media to moving stochastic vehicle loads has not yet been studied in the literature.

4.2 Problem statement of MSP

4.2.1 Pavement as a continuum medium

Pavement structures are traditionally classified into two categories: rigid pavement and flexible pavement. The former often refers to Portland cement concrete (PCC) pavement, the latter often refers to asphalt concrete (AC) pavement. This classification is not very strict because PCC pavements are not “rigid,” or are AC pavements “flexible” in many situations. From the standpoint of structural nature PCC pavements behave more like a slab, while AC pavement acts more like a multi-layered system. Therefore, it is more reasonable to classify pavement on the base of mechanic properties. There have been developed many models to simulate the behavior of pavement structures. For instance, Hardy and Cebon [16, 18] simplified AC pavement into an Euler–Bernoulli beam. From the theoretical perspective, most of the proposed pavement models belong to continuum media [102, 183–187].

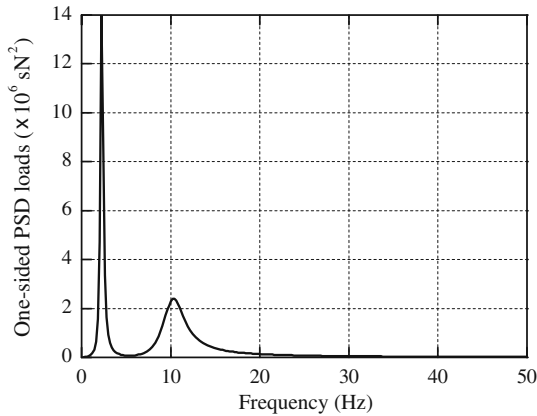


Fig. 11 PSD of contact forces against frequency (speed of travel = 20 m/s)

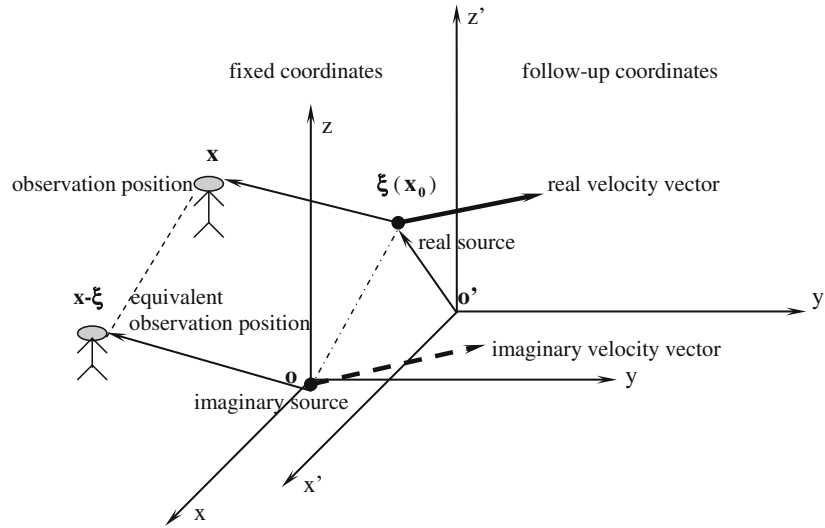


Fig. 12 Schematic sketch of a stationary coordinate and a moving coordinate

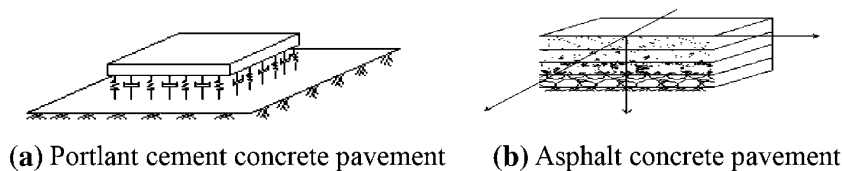


Fig. 13 Physical models of two general types of pavement structures

Consider a linear medium with the region R or the boundary B being at rest initially. A load is applied when the medium is at rest and moves according to a given law of motion (Fig. 12). The MSP is to solve the response of the medium to the moving load. The governing equation of such a system thus belongs to linear partial differential equation. According to the theory of linear equation, the solution of the equation can be constructed by the integration of the fundamental solution of the equation or the so-called Green's function. It is usually described as the superposition principle or, equivalently, the reciprocal principle [103].

Besides the above-mentioned description of the continuum media, the following assumptions are made here. One assumption is that, comparing to the mass of vehicle, the mass of pavement structures (including surface layer, base, subgrade, and soil foundation) is large enough such that pavement vibration is much smaller than vehicle vibration. Another assumption is that wave velocity excited by a dynamic load in pavement structure is much faster than vehicle's speed of travel. With these two assumptions, the couple effect of vehicle-pavement interaction can be negligible.

4.2.2 Moving stochastic vehicle loads

Contact forces applied on pavements by vehicles are moving stochastic loads. The statistical characteristics of the dynamic contact forces have been discussed in detail previously. Dynamic contact forces follow with two aspects of meanings. One is that the location of the force is changing continuously with traveling of vehicle, and another is that the amplitude of the force is varying due to vehicle vibrations.

Without any loss of generality, a vehicle is assumed to be a linear system traveling along the x -axis at a constant speed. The contact forces between the vehicle and pavement can be given by a concentrated moving load:

$$F(\mathbf{x}, t) = P_{sto}(t)\delta(x - vt)\delta(y) \quad (95)$$

where t and v are time variable and vehicle velocity, respectively, $\delta()$ is the Dirac-delta function, which is defined by

$$\delta(x - x_0) = \begin{cases} 0, & \text{for } x \neq x_0 \\ \infty, & \text{for } x = x_0 \end{cases} \text{ and } \int_{-\infty}^{\infty} f(x)\delta(x - x_0)dx = f(x_0). \quad (96)$$

In addition, $P_{sto}(t)$, a function of time, represents amplitudes of stochastic contact forces and can be expressed as two terms below:

$$P_{sto}(t) = P_0 + P(t). \quad (97)$$

Here P_0 , representing the static load applied at a tire when the vehicle is at rest, is a constant quantity, and $P(t)$ represents the dynamic portion of the stationary stochastic contact forces with a zero mean. Its correlation function, power spectral density and standard deviation are, respectively, denoted as $R_{PP}(\tau)$, $S_{PP}(\omega)$, and σ_P .

4.3 Representation theory of MSP

It is convenient to assume a three-dimensional configuration with observation variable $\mathbf{x} = (x, y, z)$, source variable $\boldsymbol{\xi} = (\xi, \eta, \zeta)$, and time $t \geq 0$. Suppose a linear differential operator \mathbf{O} describes the dynamic property of a physical system and appropriate interface and boundary conditions relate the field quantities of specified problems. Obviously, for a concrete elastodynamic problem, the linear differential operator \mathbf{O} is given by the well-known Navier-Stoke's field equations. The Green's function is then defined as the fundamental solution of the system. In other words, for the problem discussed here, the Green's function corresponds to the solution of the governing equations as the point source takes the form of a Dirac delta function in both spatial and temporal domains.

4.3.1 General Formulation

Without loss of generality, vanishing initial conditions are assumed here. According to the causality of a physical system, the Green's function $\mathbf{G}(\mathbf{x}, t) = 0$ for $t < 0$. We may then write

$$\mathbf{O}[\mathbf{G}(\mathbf{x} - \boldsymbol{\xi}, t - \tau)] = \delta(\mathbf{x} - \boldsymbol{\xi})\delta(t - \tau). \quad (98)$$

Here, the initiation of the source is delayed by τ . The causality of a physical system requires that for Green's function $t \leq \tau$. Since the initial condition of the linear medium is zero, the dynamic response could be expressed as

$$\mathbf{u}(\mathbf{x}, t) = \int_{-\infty}^t \int_S F(\boldsymbol{\xi}, \tau)\mathbf{G}(\mathbf{x}, t - \tau; \boldsymbol{\xi})d\boldsymbol{\xi}d\tau, \quad (99)$$

where $\mathbf{x} = (x, y, z)$, $\boldsymbol{\xi} = (\xi, \eta, \zeta)$, $\mathbf{v} = (v_x, v_y, v_z)$, $d\boldsymbol{\xi} = d\xi d\eta d\zeta$, and S is the region R or the boundary B . It is known that the Green's function $\mathbf{G}(\mathbf{x}, t; \boldsymbol{\xi})$ corresponds to the solution of the equation when a unit point impulse is applied at position $\boldsymbol{\xi}$. Assume that the medium is infinite in those dimensions of interest. It is known that the governing equations are linear. According to the reciprocal principle, the response of media at field point \mathbf{x} in the fixed coordinates when the source lies at $\boldsymbol{\xi}$ in the fixed coordinates is equal to the response of media at field point $\mathbf{x} - \boldsymbol{\xi}$ in the fixed coordinates when the source lies at $\mathbf{0}$ in the same coordinate.

Define the impulse response function (IRF) $\mathbf{h}(\mathbf{x}, t)$ as the solution of

$$\mathbf{O}[\mathbf{h}(\mathbf{x}, t - \tau)] = \delta(\mathbf{x})\delta(t - \tau). \tag{100}$$

According to the above mentioned analysis, we have

$$\mathbf{h}(\mathbf{x} - \boldsymbol{\xi}, t) = \mathbf{G}(\mathbf{x}, t; \boldsymbol{\xi}) = \mathbf{G}(\mathbf{x} - \boldsymbol{\xi}, t; \mathbf{0}). \tag{101}$$

Substituting (101) into (99), we get

$$\mathbf{u}(\mathbf{x}, t) = \int_{-\infty}^t \int_S F(\boldsymbol{\xi}, \tau) \mathbf{h}(\mathbf{x} - \boldsymbol{\xi}, t - \tau) d\boldsymbol{\xi} d\tau. \tag{102}$$

Furthermore, if the concrete form $F(\boldsymbol{\xi}, \tau)$ in (103) is considered, we may rewrite (102) as

$$\mathbf{U}(\mathbf{x}, t) = \int_{-\infty}^t P_{sto}(\tau) \mathbf{h}(\mathbf{x} - \mathbf{v}\tau, t - \tau) d\tau. \tag{103}$$

in which $\mathbf{v}\tau = (v_x\tau, v_y\tau, v_z\tau)$. Also, the property of Dirac delta function (102) is used here. If the transformation $\theta = t - \tau$ is used, then (103) can be expressed as

$$\mathbf{u}(\mathbf{x}, t) = \int_0^{\infty} P_{sto}(t - \theta) \mathbf{h}(\mathbf{x} - \mathbf{v}t + \mathbf{v}\theta, \theta) d\theta. \tag{104}$$

Equations (103) and (104) are general results for MSP and are named generalized Duhamel’s integral (GDI). From the point of view of time history, we might regard a moving load as a series of impact on continuum media during a number of tiny time intervals. The integration of the response of the medium excited by each impulse is thus equal to the cumulative effect of the moving load. Although solving for the Green’s function is still a nontrivial task, convolution (103) does provide a sound theoretical representation, which can be very powerful when combining with numerical computation such as finite element method.

4.3.2 Deterministic analysis for a moving constant load

The solution of the problem described here can be constituted using the solutions of two individual problems because of the superposition principle of the solution of linear equations. One problem deals with the deterministic response of the medium under the moving constant load $P_0\delta(x - vt)\delta(y)$. The other problem deals with the random response of the medium under the moving stochastic load $P(t)\delta(x - vt)\delta(y)$. In this section, the first problem is analyzed. In the next section, the second problem is analyzed. The summary of the solution is provided in the sections followed. If the load is a constant with amplitude P_0 , the response are given by

$$\mathbf{u}(\mathbf{x}, t) = P_0 \int_0^{\infty} \mathbf{h}(x - vt + v\theta, y, z, \theta) d\theta. \tag{105}$$

It is obvious that the response is no longer a constant independent on the time t . If the source is a fixed load, according to our example, the solution should be a static

quantity. Actually, this idea is straightforward demonstrated by putting the velocity variable $v = 0$ into (105). The result gives that

$$\mathbf{u}(\mathbf{x}, t) = P_0 \int_0^{\infty} \mathbf{h}(\mathbf{x}, \theta) d\theta. \tag{106}$$

Clearly, the response is a constant without depending on the time variable.

4.3.3 Stochastic analysis for a moving stochastic vehicle load

In this section, a stochastic moving source is analyzed. In the derivation of the GDI in (103), we require no special assumptions on $P_{sto}(t)$. Therefore, if $P_{sto}(t)$ is a stochastic process, and (103) becomes an integral in the sense of Stieltjes integration. Meanwhile, the response $\mathbf{u}(\mathbf{x}, t)$ becomes a stochastic process. We now consider the response of media to $P(t)\delta(x - vt)\delta(y)$.

As mentioned before, $P(t)$ is a zero mean stationary process with autocorrelation function $R_{PP}(\tau)$, PSD $S_{PP}(\omega)$ and standard deviation σ_P . Taking the expectation of both sides of (103) and using the exchangeability of expectation and integration, we obtain the mean function of the response, i.e.,

$$\mathbf{u}(\mathbf{x}, t) = \int_0^{\infty} E[P(t - \theta) \mathbf{h}(x - vt + v\theta, y, z, \theta)] d\theta. \tag{107}$$

It is not difficult to obtain the spatial-time correlation functions for the response, i.e.,

$$\begin{aligned} R_{\mathbf{u}}(\mathbf{x}_1, \mathbf{x}_2; t_1, t_2) &= \int_{-\infty}^{t_2} \int_{-\infty}^{t_1} E[P(\tau_1)P(\tau_2) \mathbf{h}(x_1 - v\tau_1, y_1, z_1, t_1 - \tau_1) \\ &\quad \times \mathbf{h}(x_2 - v\tau_2, y_2, z_2, t_2 - \tau_2)] d\tau_1 d\tau_2, \end{aligned} \tag{108}$$

where $R_{\mathbf{u}}(\mathbf{x}_1, \mathbf{x}_2; t_1, t_2)$ is the correlation function of response $\mathbf{u}(\mathbf{x}, t)$. Let $\mathbf{x}_1 = \mathbf{x}_2 = \mathbf{x}$, then we obtain the time autocorrelation function

$$\begin{aligned} R_{\mathbf{u}}(\mathbf{x}; t_1, t_2) &= \int_0^{\infty} \int_0^{\infty} E[P(t_1 - \theta_1)P(t_2 - \theta_2) \\ &\quad \times \mathbf{h}(x - vt_1 + v\theta_1, y, z, \theta_1) \\ &\quad \times \mathbf{h}(x - vt_2 + v\theta_2, y, z, \theta_2)] d\theta_1 d\theta_2. \end{aligned} \tag{109}$$

where $\theta_j = t_j - \tau_j (j = 1, 2)$. By substituting $t_1 = t_2 = t$ into (108) and (109), it is straightforward to find second moment functions, i.e., the mean square functions of the random response.

It has been known that for a linear system with a stationary stochastic excitation at a fixed position, the response of that system is still a stationary stochastic process [76]. However, this conclusion only applies to the fixed source problem. For a linear system with a moving stochastic source, the random response of that system is a nonstationary stochastic process

even if the random excitation $P(t)$ is a stationary stochastic process [54, 74]. To show this, we inspect (107) and (109), which are apparently not stationary because time variable t is contained in the kernel function of the solution. In other words, in a situation where a source is moving with respect to a receiver a nonstationary signal will be recorded at the observer position, even when the source produces a stationary output. This effect is known as the Doppler shift. It is also useful to realize that although the system is a linear system, it essentially becomes a time varying system when a moving source is applied.

In many circumstances, there may be a demand to push the analysis further into the frequency domain. For instance, response information of amplitude distributions and frequency components of media to moving vehicle loads is needed for vehicle optimum control and pavement performance prediction. To fulfill this purpose, it is necessary to use spectral analysis techniques to obtain the required information. As such, one may encounter difficulties when performing Fourier spectral analysis technique because this technique has been devised primarily for stationary signals. Although some variations of Fourier spectral analysis technique have been introduced to dealing with nonstationary stochastic processes, Fourier spectral analysis are not ideal tools for nonstationary signals induced by MSP. This shortcoming has led Sun [104] to develop the so-called follow-up spectral analysis, by which the commonly used spectral analysis technique is still applicable with sound theoretical foundation.

Let coordinates $oxyz$ and $o'x'y'z'$ be, respectively, fixed coordinates and follow-up coordinates moving with the moving source. The relationship between the two coordinates is

$$\mathbf{x}' = \mathbf{x} - \mathbf{v}t. \quad (110)$$

Therefore, a moving source $\mathbf{x}_0 + \mathbf{v}t$ in the fixed coordinate $oxyz$ becomes a fixed source $\mathbf{x}' = \mathbf{x}_0$ in the follow-up coordinate $o'x'y'z'$. Here \mathbf{x}_0 is a constant vector. Now consider the response of the medium at a moving field point $\mathbf{x} + \mathbf{v}t + \mathbf{x}_0$ in the fixed coordinates. Utilizing (104), we have

$$\mathbf{u}(\mathbf{x} + \mathbf{v}t + \mathbf{x}_0, t) = \int_0^\infty P_{sto}(t - \theta) \mathbf{h}(\mathbf{x} + \mathbf{x}_0 + \mathbf{v}\theta, \theta) d\theta. \quad (111)$$

The mean function and autocorrelation function of the response described by (111) are, respectively, given by

$$\begin{aligned} E[\mathbf{u}(\mathbf{x} + \mathbf{v}t + \mathbf{x}_0, t)] &= \int_0^\infty E[P_{sto}(t - \theta) \mathbf{h}(\mathbf{x} + \mathbf{x}_0 + \mathbf{v}\theta, \theta)] d\theta \\ &= E[P_{sto}(t - \theta)] \int_0^\infty \mathbf{h}(\mathbf{x} + \mathbf{x}_0 + \mathbf{v}\theta, \theta) d\theta \\ &= P_0 \int_0^\infty \mathbf{h}(\mathbf{x} + \mathbf{x}_0 + \mathbf{v}\theta, \theta) d\theta. \end{aligned} \quad (112)$$

and

$$\begin{aligned} R_{\mathbf{u}}(\mathbf{x} + \mathbf{v}t + \mathbf{x}_0, \tau) &= \int_0^\infty \int_0^\infty R_{PP}(\tau + \theta_1 - \theta_2) \mathbf{h}(\mathbf{x} + \mathbf{x}_0 + \mathbf{v}\theta_1, \theta_1) \\ &\quad \times \mathbf{h}(\mathbf{x} + \mathbf{x}_0 + \mathbf{v}\theta_2, \theta_2) d\theta_1 d\theta_2. \end{aligned} \quad (113)$$

According to the definition of a stationary stochastic process [31], (112), and (113) indicate that the response at a moving field point $\mathbf{x} + \mathbf{v}t + \mathbf{x}_0$ in the fixed coordinates becomes a stationary process. It is evident that the moving field point $\mathbf{x} + \mathbf{v}t + \mathbf{x}_0$ in the fixed coordinates becomes a fixed field point $\mathbf{x} + \mathbf{x}_0$ in the follow-up coordinates as illustrated in Fig. 12. To show this, we replace \mathbf{x} in (110) by $\mathbf{x} + \mathbf{v}t + \mathbf{x}_0$

$$\mathbf{x}' = \mathbf{x} + \mathbf{x}_0. \quad (114)$$

In other words, the response of a fixed position $\mathbf{x} + \mathbf{x}_0$ in the follow-up coordinates to a moving stationary stochastic load possesses the stationary property. Thus, Fourier spectral analysis technique is still applicable here. It should be pointed out that the explanation of the stationary process $\mathbf{u}(\mathbf{x} + \mathbf{v}t + \mathbf{x}_0, t)$ is essentially different from the commonly described stationary process. In general, the mean function of a commonly described stationary process refers to the time average of the random process, while the mean in (112) is indeed interpreted as a spatial average of the random response. The same explanation applies to the autocorrelation function shown in (113).

In light of the aforementioned explanation, there is no difficulty to define PSD in the follow-up coordinates. The following spectral analysis is performed in the follow-up coordinates. We may rewrite the autocorrelation function in the follow-up coordinates as

$$\begin{aligned} R_{\mathbf{u}}(\mathbf{x}', \tau) &= \int_0^\infty \int_0^\infty R_{PP}(\tau + \theta_1 - \theta_2) \mathbf{h}(\mathbf{x} + \mathbf{x}_0 + \mathbf{v}\theta_1, \theta_1) \\ &\quad \times \mathbf{h}(\mathbf{x} + \mathbf{x}_0 + \mathbf{v}\theta_2, \theta_2) d\theta_1 d\theta_2, \end{aligned} \quad (115)$$

where \mathbf{x}' is expressed by (114). Let $\tau = 0$ and put it into Eq. (115), we obtain the mean square function of the random response in the follow-up coordinate

$$\begin{aligned} \psi_{\mathbf{u}}^2(\mathbf{x}', t) &= \int_0^\infty \int_0^\infty \psi_p^2(\theta_2 - \theta_1) \mathbf{h}(\mathbf{x} + \mathbf{x}_0 + \mathbf{v}\theta_1, \theta_1) \\ &\quad \times \mathbf{h}(\mathbf{x} + \mathbf{x}_0 + \mathbf{v}\theta_2, \theta_2) d\theta_1 d\theta_2. \end{aligned} \quad (116)$$

In addition, since $P(t)$ is a zero mean stationary process, we have

$$\sigma_p^2 = \text{Var}[P(t)] = \psi_p^2 = R_{PP}(0) = \text{const}, \quad (117)$$

where σ_p and $\text{Var}[P(t)]$ are, respectively, the standard deviation and variance of $P(t)$. So we can rewrite (117) as

$$\sigma_{\mathbf{u}}^2(\mathbf{x}', t) = \psi_{\mathbf{u}}^2(\mathbf{x}', t) = \left[\int_0^\infty \mathbf{h}(\mathbf{x} + \mathbf{x}_0 + \mathbf{v}\theta, \theta) d\theta \right]^2 R_{PP}(0), \tag{118}$$

where $\sigma_{\mathbf{u}}$ and $\psi_{\mathbf{u}}^2$ are the standard deviation and variance of the response field, respectively. Define the relationship between the frequency response function and the impulse unit response function in the follow-up coordinates as

$$\mathbf{H}(\mathbf{x}'; \omega) = \int_0^\infty \mathbf{h}(\mathbf{x} + \mathbf{x}_0 + \mathbf{v}\theta, \theta) e^{-i\omega\theta} d\theta. \tag{119}$$

According to Wiener-Khintchine theory, the PSD and the autocorrelation function form a Fourier transform pair. Taking Fourier transform to both sides of (115) and noticing the (119), we obtain the expression of PSD in follow-up coordinates, i.e.,

$$S_{\mathbf{u}}(\mathbf{x}'; \omega; \mathbf{v}) = |\mathbf{H}(\mathbf{x}'; \omega)|^2 S_{PP}(\omega). \tag{120}$$

Similarly, an expression for the time autocorrelation function can be obtained by taking the Fourier inverse transform of (120)

$$R_{\mathbf{u}}(\mathbf{x}'; \tau) = (2\pi)^{-1} \int_{-\infty}^\infty |\mathbf{H}(\mathbf{x}'; \omega)|^2 S_{PP}(\omega) e^{i\omega\tau} d\omega. \tag{121}$$

Hence, the mean square function is also given by

$$\psi_{\mathbf{u}}^2(\mathbf{x}') = R_{\mathbf{u}}(\mathbf{x}'; \tau) = (2\pi)^{-1} \int_{-\infty}^\infty |\mathbf{H}(\mathbf{x}'; \omega)|^2 S_{PP}(\omega) d\omega. \tag{122}$$

4.4 Pavement Models

There are mainly two types of pavement structures: Portland cement concrete pavement and asphalt concrete pavement (Fig. 13). These pavement structures can be modeled by a beam, a slab, a layered medium on a half-space or rigid bedrock. A number of studies have been carried out lately by Sun and his associates using analytic method and analytic–numerical method [105–163]. Beskou and Theodorakopoulos [164] provided a recent review on numerical methods for studying dynamic effects of moving loads on road pavements. Sun and Greenberg [74], Sun and Luo [125–128], Sun et al. [153], Luo et al. [165] and Sun et al. [123] provide concrete examples of pavement models subject to moving loads.

The response of pavement systems under dynamic loads may be expressed in partial-differential equations. A generic description of the governing equations is:

$$\varphi[\mathbf{u}(\mathbf{x}, t; \theta)] = \mathbf{P}(\mathbf{x}, t), \tag{123}$$

where $\varphi[\cdot]$ is a partial-differential operator, $\mathbf{x} = (x, y, z)$ a spatial vector in Cartesian coordinates, t is the time variable, $\mathbf{P}(\mathbf{x}, t)$ is the applied dynamic load (i.e., the input),

which can be recorded by data acquisition system during laboratory experiments and field tests, $\mathbf{u}(\mathbf{x}, t; \theta)$ the pavement response vector (i.e., the output in the form of displacements, stresses, and strains), and $\theta = (\theta_1, \theta_2, \dots, \theta_n)$ is the parameter vector to be identified.

A pavement structure usually consists of a surface course, base courses and subgrade. Within each course, there may be several sub-layers made up of different materials. A two-dimensional Kirchhoff thin slab resting on a Winkler foundation is the common model for PCC pavements. The operator $\varphi[\cdot]$ for a Kirchhoff thin slab is

$$\varphi[\cdot] = D\nabla^2\nabla^2 + K + C\partial/\partial t + \rho h\partial^2/\partial t^2, \tag{124}$$

where $D = Eh^3/[12(1 - \mu^2)]$, and ρ, μ and h are the density, Poisson’s ratio and thickness of the slab, E is the Young’s elastic modulus, K is the modulus of subgrade reaction, C is the radiation damping coefficient, and $\nabla^2 = \partial^2/\partial x^2 + \partial^2/\partial y^2$ is the Laplace operator. The parameter vector is $\theta = (E, h, \mu, K, C, \rho)$. For a multilayered flexible pavement system, the governing equation is controlled by a three-dimensional Navier–Stokes’s equation for each layer

$$G^*\nabla^2\mathbf{u} + (\lambda^* + G^*)\nabla\nabla \cdot \mathbf{u} + \rho\mathbf{f} = \rho\partial^2\mathbf{u}/\partial t^2, \tag{125}$$

where $\nabla = \partial/\partial x + \partial/\partial y + \partial/\partial z$, \mathbf{f} the body force vector, the Laplace operator $\nabla^2 = \partial^2/\partial x^2 + \partial^2/\partial y^2 + \partial^2/\partial z^2$, $G^* = G(1 + i\eta_d)$, $\lambda^* = \lambda(1 + i\eta_d)$ in which $i = \sqrt{-1}$, η_d is the hysteretic damping coefficient, Lamb constants λ and G the bulk modulus and shear modulus, respectively, λ^* and G^* the complex counterparts of λ and G , respectively. The subgrade may be artificially divided into a number of thin layers. Within each layer the soil is characterized to be isotropic, homogenous and have the same structural and material properties, while these properties vary for different layers. Furthermore, physical nonlinearity may possibly be presented in asphalt surface layer and soil subgrade using nonlinear constitutive models involving viscoelasticity-viscoplasticity. Eq. (125) adopts the simplest model to account for viscoelasticity. A more generic model is the generalized viscoelastic model, which includes the Burgers model, Maxwell model and Kelvin model as its special cases. Fig. 14 presents a schematic plot of a list of viscoelastic models.

To solve a viscoelastic problem, elastic solutions is sought first and then the correspondence principle is applied to convert the elastic solution into a viscoelastic solution. Two elastic/viscoelastic subgrade models will be studied: a half-space and a layer resting on bedrock. Clearly, the parameter vector $\theta = (E, h, \lambda, G, \rho)$ varies from layer to layer. When viscoelasticity is considered, more parameters will appear in the parameter vector. In principle, the adoption of a generalized viscoelastic model in forward dynamic analysis introduces no significant

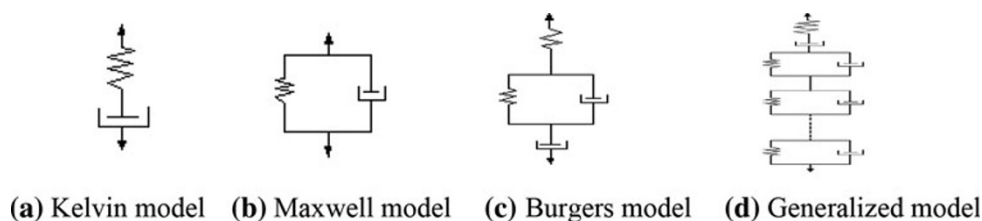


Fig. 14 A schematic plot of different viscoelastic models

difficulty. The number of Kelvin components in this model can be estimated through a thorough investigation. With properly specified initial and boundary conditions, Eqs. (123)–(125) constitute a complete mathematical description of the forward dynamic problem. Forward analysis aims to solve for the response $\mathbf{u}(\mathbf{x}, t; \theta)$ provided that the excitation $\mathbf{P}(\mathbf{x}, t)$ and the parameter vector θ are known. These mathematical, physical models describe the behavior of different types of pavement systems and they will be studied in great depth.

Equation (123) belongs to a wave equation from a mathematical physics point of view. Its solution can be obtained in the form of a Lebesgue–Stieltjes integral using proper integral transformation, depending upon the nature of the problem (e.g., steady-state vs. transient) and upon how the problem is formulated (e.g., in Cartesian or cylindrical coordinates). Let the Green’s function (the fundamental solution) of Eq. (1) be $\mathbf{G}(\mathbf{x}, t; \theta) = \varphi^{-1}[\delta(\mathbf{x}, t)]$, in which $\delta(\cdot)$ is the Dirac-delta function and $\varphi^{-1}[\cdot]$ denotes the inverse operator of $\varphi[\cdot]$. Let pavements be at rest prior to the NDE test, leading to a vanishing initial condition. The solution of Eq. (123) under loading condition $\mathbf{P}(\mathbf{x}, t)$ can be constructed as

$$\mathbf{u}(\mathbf{x}, t; \theta) = \varphi^{-1}[\mathbf{P}(\mathbf{x}, t)] = \int_S \mathbf{G}(\mathbf{x}, t; \theta) dS, \tag{126}$$

where S is the region where $\mathbf{P}(\mathbf{x}, t)$ is defined. Equation (126) can also be equivalently represented in the transformed domain

$$\tilde{\mathbf{u}}(\boldsymbol{\xi}, \omega; \theta) = T\{\{\mathbf{u}(\mathbf{x}, t; \theta)\}\} = \int_{\tilde{S}} \tilde{\mathbf{G}}(\boldsymbol{\xi}, \omega; \theta) d\tilde{S}, \tag{127}$$

where $T\{\cdot\}$ is a transformation operator, $\tilde{\mathbf{u}}(\boldsymbol{\xi}, \omega; \theta)$ and $\tilde{\mathbf{G}}(\boldsymbol{\xi}, \omega; \theta)$ are the response and the Green’s function in the transformed domain, respectively, \tilde{S} is the region in the transformed domain where the transformed dynamic load $\tilde{\mathbf{P}}(\boldsymbol{\xi}, \omega)$ is defined; $\boldsymbol{\xi} = (\xi, \eta, \zeta)$ and ω are the counterpart of spatial vector $\mathbf{x} = (x, y, z)$ and time variable t .

The Thomas-Haskell method relates a transformed response at the bottom of a layer, in the form of a transfer matrix, to a corresponding quantity at the top of a lower layer. For the last half century, this method has served as the

cornerstone for numerous studies in multilayered elastic analysis. Another benchmark proposed by Kausel and Roesset contributes an alternative, in which the dynamic stiffness matrix is expanded in terms of wave number and approximated by taking terms only up to the second order of the wave number. The Thomas-Haskell method is more accurate than the Kausel-Roesset method but demands more computational effort. Forward dynamic analysis for multilayered viscoelastic media will not add significant difficulty because both methods are still applicable, though it is a demanding task. Since each method has its own strengths and weaknesses, both methods will be adopted in the project to tackle wave propagation through multilayered viscoelastic media. Equations (126) and (127) are amenable to numerical evaluation of the dynamic response in the time-space domain and in the transformed domain, respectively, provided that $\mathbf{P}(\mathbf{x}, t)$ and θ are known. Without doubt, the computation here involves intensive numerical evaluation of multifold integration of complex functions with unstable characteristics in time and space.

5 Discussion and Future Research

In this section, discussion and future research of the unified theory of dynamics of vehicle–pavement interaction under moving and stochastic load is carried out from the following aspects: (a) nature of the problem, (b) modeling, (c) methodology, and (d) further extension and engineering application.

(a) Nature of the problem. The setting of vehicle–pavement interaction can be categorized either in a deterministic framework or a stochastic framework. Stochasticity may be presented in speed, magnitude and position of the loading, structural models of vehicle–pavement system and constitutive models. A stochastic framework provides a more realistic setting but exhibit more complexity. The setting of vehicle–pavement interaction can also be categorized either as a steady-state problem or as a transient problem. Except very few studies [104, 145], almost all existing literatures belong to a steady-state problem described in a deterministic framework.

(b) **Modeling.** The modeling of vehicle–pavement interaction involves the load model, the vehicle model and the pavement model. The load model addresses spatial distribution of the load (e.g., concentrated load, distributed load, multiple load, etc.), speed of the load (e.g., constant speed, varying speed, etc.), trajectory of the load (e.g., straight line, curve, etc.), and magnitude of the load (e.g., constant load, impact load, sinusoidal load, varying load, and random load). The vehicle model addresses vehicle suspension system, which involves mass distribution, dimension, and configuration of the vehicle. Quarter-vehicle model, half-vehicle model, and whole vehicle model have all been established with increasing complexity involving different number of spring and dashpot elements. Regardless of how many spring and dashpot elements are being used in the built vehicle model, almost all the literature studies tend to use linear suspension system due to its ease of computation when integrated with a pavement model. The pavement model addresses the simplification of structural system of pavement using beam model, slab model, and layered medium on a half space or bedrock. In terms of constitutive models of the material, almost all studies only considered linear elastic and linear viscoelastic materials when tackling dynamics of vehicle–pavement interaction because of the complexity of the problem. Asphalt concrete pavement actually exhibits complex viscoelastic–viscoplastic–damage properties [166–172], which should be integrated into the subject. Also, it is rare to consider the coupling effect of vehicle–pavement interaction, while this is not the case in train–railway interaction because of the mechanism of the interaction and the relative mass difference between vehicles (e.g., car, truck, train, and airplane) and transportation infrastructure (e.g., highway, bridge, and railway). None of the studies has addressed vehicle–pavement interaction using deteriorated pavement models as well as long-term pavement damage and failure due to vehicle–pavement interaction.

(c) **Methodology.** The methods for solving vehicle–pavement interaction problem can be classified into analytic approach and numerical application, though the implementation of analytic approach still requires numerical computation. For vehicle dynamics, equation of motion is first established as a set of linear differential equation system and solved in the frequency domain using frequency response function or in the time domain using numerical sequential integration. For pavement dynamics, analytic approach makes use of integral transform to treat wave propagation in continuum media, while numerical approach such as finite difference, finite element and boundary element methods makes use of discretization in time and in space. The advantage of analytic approach is that it provides insights for revealing physics of the wave propagation in continuum media and can be highly efficient

in terms of computation implementation, particularly when the spatial scale of the problem involves hundreds of kilometers (e.g., seismology) or the speed of the load is very high and close to various critical speeds of waves in media. The advantage of numerical approach is that they can deal with pavement having complex geometric structure as well as nonlinear constitutive model of the material.

(d) **Further extension and engineering application.** The study of dynamics of vehicle–pavement interaction provides a deep understanding for improving vehicle design (e.g., road-friendly vehicle suspension system), road transportation safety [173–177], long-lasting pavement structures design [178–181], ride quality and infrastructure asset management. An improved quantitative understanding on effects and mechanisms of various factors on dynamics of vehicle–pavement interaction is the fundamentals for increased application and accuracy and reliability of structural health monitoring, nondestructive testing and evaluation, environmental vibration mitigation and weight-in-motion. It will also benefit the nation’s transportation economy by reducing operation and maintenance costs of vehicles and transportation infrastructure as well as increasing transportation productivities.

6 Conclusions

Irregularities of pavement surface, from the small-scale unevenness of material on pavement surface to the large-scale undulating of vertical curve of a highway or an airport, all belong to spatial fluctuation of pavement surface at different scale. Extensive study has been accomplished both domestically and internationally, toward measuring the physical aspects of pavement roughness, analyzing the resulting data, and evaluating the riding performance of pavements. Instrumentation and analysis technique including the spectral analysis approaches have been summarized in the article. A number of the PSD functions including the effect of thermal joints on PSD roughness have been presented here. These PSD functions are similar in their shapes and only different in their mathematical descriptions. Under the condition of constant speed of travel and linear vehicle suspension, it is proven that dynamic contact force between vehicle and pavement is a stationary stochastic process. Its mean function is given by (79) without the consideration of static loads or by (80) with the consideration of static loads. The correlation function, PSD forces, and standard deviation are, respectively, given by (84), (89) and (92). The concept and the methodology present in the article are not restricted to specific surface roughness and/or vehicle models. They are generally applicable to all kinds of linear vehicle models and measured pavement surface conditions. The response

of linear continuum media to moving stochastic vehicle loads is analyzed herein. We show that there exists predictable relation among surface roughness, vehicle suspensions and speed, and the response of continuum media. The theory developed here is widely applicable to moving vehicle loads.

Acknowledgments This study is sponsored in part by the National Science Foundation, by National Natural Science Foundation of China, by Ministry of Communication of China, by Jiangsu Natural Science Foundation to which the author is very grateful. The author is also thankful to Professor Wanming Zhai, Editor Mr. Yao Zhou and Editor-in-Chief Yong Zhao for their invitations.

Open Access This article is distributed under the terms of the Creative Commons Attribution License which permits any use, distribution, and reproduction in any medium, provided the original author(s) and the source are credited.

References

- Pavement Roughness and Rideability, Project 1–23 (1981) National Cooperative Highway Research Program, Project Statement
- Abbo E, Hedric JK, Markow M, Brademeyer B (1987) Analysis of moving loads on rigid pavements. International symposium on heavy truck suspensions, Canberra, Australia
- Hudson WR et al. (1992) Impact of truck characteristics on pavements: truck load equivalent factors. Report No. FHWA-RD-91-064, Federal Highway Administration, Washington, DC
- Gillepie TD et al. (1993) Effects of heavy-vehicle characteristics on pavement response and performance, Report 353, National Cooperative Highway Research, National Academy Press, Washington, DC
- Barrodal I, Erickson RE (1980) Algorithms for least-square linear prediction and maximum entropy spectral analysis. *Geophysics* 45:420–446
- Bendat JS, Piersol AG (1971) *Random data: analysis and measurement procedure*. Wiley-Interscience, New York
- Beskou ND, Theodorakopoulos DD (2011) Dynamic effects of moving loads on road pavements: a review. *Soil Dyn Earthq Eng* 31(4):547–567
- BSI proposals for generalized road inputs to vehicles (1972) *ISO/TC, 108/WG9*, document no. 5, International Organization for Standardization
- Captain KE, Boghani AB, Wormley DN (1979) Analytical tire models for dynamic vehicle simulation. *Veh Syst Dyn* 8:1–32
- Cebon D (1989) Vehicle-generated road damage: a review. *Veh Syst Dyn* 18(1–3):107–150
- Cebon D (1993) Interaction between heavy vehicles and roads. *SAE Technical Paper No. 93001*, Society of Automotive Engineers
- Chen, S.S. (1987). The response of multi-layered systems to dynamic surface loads. Ph.D Dissertation, Department of Civil Engineering, University of California, Berkeley, California
- Cole DJ (1990) Measurement and analysis of dynamic tire forces generated by lorries. Ph.D Dissertation, University of Cambridge, Cambridge United Kingdom
- Cole J, Huth J (1958) Stresses produced in a half-plane by moving loads. *J Appl Mech*, ASME 25:433–436
- De Barro FCP, Luco JE (1994) Response of a layered viscoelastic half-space to a moving point load. *Wave Motion* 19(2):189–210
- Deng X and Sun L (1996) Dynamic vertical loads generated by vehicle–pavement interaction. CSME 12th proc. symp. on advances in transportation system, Canadian Society for Mechanical Engineering, Hamilton
- Deng X, Sun L (1996) The Euclid norm weight model for and its application in pavement evaluation. *China J Highw Transp* 9(1):21–29
- Dodds CJ (1974) The laboratory simulation of vehicle service stress. *J Eng Ind Trans*, ASME 96(3):391–398
- Dodds CJ, Robson JD (1973) The description of road surface roughness. *J. Sound Vib* 31:175–183
- Eason G (1965) The stresses produced in a semi-infinite solid by a moving surface force. *Int J Eng Sci* 2:581–609
- Elattary MA (1991) Moving loads on an infinite plate strip of constant thickness. *J Phys D* 24(4):541–546
- Eringen AC, Suhubi ES (1975) *Elastodynamics*, vol I. Academic Press, New York
- Felszegpy SF (1996) The Timoshenko beam on an elastic foundation and subject to a moving step loads, Part I: steady-state response. *J Vib Acous*, ASME 118:227–284
- Felszegpy SF (1996) The Timoshenko beam on an elastic foundation and subject to a moving step loads, Part II: transient response. *J Vib Acous*, ASME 118:285–291
- Fryba L (1972) *Vibration of solids and structures under moving loads*. Noordhoff International Publishing, Gronigen
- Fryba L, Nakagiri S And, Yoshikawa N (1993) Stochastic finite elements for a beam on a random foundation with uncertain damping under a moving force. *J Sound Vib* 163(1):31–45
- Gakenheimer DC, Miklowitz J (1969) Transient excitation of an elastic half space by a point load traveling on the surface. *J Appl Mech*, ASME 37:505–522
- Galaitis AG, Bender EK (1976) Wheel/rail noise, part V: measurement of wheel and rail roughness. *J Sound Vib* 46:437–451
- Gelfand JM, Shilov GE (1964) *Generalized functions*. Volume I: properties of operations. Academic Press, New York
- Gillespie TD (1985) *Heavy truck ride: SP-607*. Society of Automotive Engineers, Warrendale
- Gillespie TD (1986) Developments in road roughness measurement and calibration procedures. University of Michigan Transportation Research Institute, Ann Arbor
- Hall AW, Hunter PA, Morris GJ (1971) Status of research on runway roughness. Report SP-270, National Aeronautics and Space Administration, p 127–142
- Hardy MSA, Cebon D (1993) Response of continues pavement to moving dynamic loads. *J Eng Mech*, ASCE 119(9):1762–1780
- Hardy MSA, Cebon D (1994) Importance of speed and frequency in flexible pavement response. *J Eng Mech*, ASCE 120(3):463–482
- Harrison RF, Hammond KJ (1986) Approximate, time domain, non-stationary analysis of stochastically excited, non-linear systems with particular reference to the motion of vehicles on rough ground. *J Sound Vib* 105(3):361–371
- Hass R, Hudson WR, Zaniewski J (1994) *Modern pavement management*. Kriger, Malabar
- Heath AN (1987) Application of the isotropic road roughness assumption. *J Sound Vib* 115(1):131–144
- Heath AN, Good MG (1985) Heavy vehicle design parameters and dynamic pavement loading. *Australian Road Research*, 15(4)
- Hedric JK and Markow M (1985) Predictive models for evaluating load impact factors of heavy trucks on current pavement conditions, Interim Report to USDOT Office of University Research under Contract DTRS5684-C-0001
- Honda H, Kajikawa Y, Kobori T (1982) Spectra of surface roughness on bridge. *J Struct Eng*, ASCE, 108(ST9), 1956–1966

41. Houbolt JC (1962) Runway roughness studies in aeronautical fields. Paper No. 3364, ASCE, New York
42. Hsueh TM, Panzani J (1974) Dynamic response of airplanes in ground operation. *J Transp Eng ASCE* 100:743–756
43. Huang YH (1993) Pavement analysis and design. Englewood Cliffs, New Jersey
44. Hudson WR and Senvner FH (1962) AASHO road test principal relationships—performance versus stress, Rigid Pavement, Special Report, Highway Research Board
45. Hwang ES, Nowak AS (1991) Simulation of dynamic load for bridges. *J Struct Eng ASCE* 117(5):1413–1434
46. Iyengar RN, Jaiswal OR (1995) Random field modeling of railway track irregularities. *J Transp Eng, ASCE*, 121(4): 303–308
47. Kamesh KM, Robson JD (1978) The application of the isotropic road roughness assumption. *J Sound Vib* 57:80–100
48. Kenney JT (1954) Steady-state vibration of beam on elastic foundation for moving load. *J Appl Mech, ASME* 21(4):359–364
49. La Barre RP, Forkes RT (1969) The measurement and analysis of road surface roughness. MIRA Report No. 1970/5
50. Lee HP (1994) Dynamic response of a beam with intermediate point constrains subject to a moving load. *J Sound Vib* 171(3):361–368
51. Lee HR, Scheffel JL (1968) Runway roughness effects on new aircraft types. *J Aerosp Eng, ASCE* 94(AT1):1–17
52. Lighthill MJ (1958) Introduction to Fourier analysis and generalized functions. Cambridge University Press, London
53. Luo F, Sun L, Gu W (2011) Elastodynamic inversion of multilayered media via surface deflection—Part II: implementation and numerical verification. *J Appl Mech* 78(5):169–206
54. Macvean DB (1980) Response of vehicles accelerating on a random profile. *Ingenieur-Archiv* 49:375–380
55. Marcondes J, Burgess GJ, Harichandran R, Snyder MB (1991) Spectral analysis of highway pavement roughness. *J Transp Eng, ASCE* 117(5):540–549
56. Marcondes JA, Snyder MB, Singh SP (1992) Predicting vertical acceleration in vehicles through road roughness. *J Transp Eng ASCE* 118(1):33–49
57. Markow M, Hdrick JK, Bradmeyer BD, Abbo E (1988) Analyzing the interactions between vehicle loads and highway pavements, paper presented at the 67th Annual meeting, Transp Res Board, Washington, DC
58. Markow M, Hedrick JK, Bradmeyer B, Abbo E (1988) Analyzing the interaction between vehicle loads and highway pavements. Paper Presented at 67th Annual Meeting of the Transportation Research Board, Washington, DC
59. McCullough BF, Steitle DC (1975) Criteria development to evaluation runway roughness. *J Transp Eng ASCE* 101(TE2): 345–363
60. Monismith CL, Mclean DB (1971) Design considerations for asphalt pavements. Report No. TE 71-8, Institute of Transportation and Traffic Engineering, University of California, Berkeley
61. Monismith CL, Lysmer J, And Sousa J, Hedrick JK (1988) Truck pavement interactions—requisite research. *Transc SAE SP-765 881849:87–96*
62. Monismith CL, Sousa J, Lysmer J (1988) Modern pavement design technology including dynamic load conditions, SAE conference on vehicle/pavement interaction, SAE Trans, Society of Automotive Engineers. SP-765, No. 881856, 33–52
63. Morse PM, Keshbach H (1953) Methods of theoretic physics. Part I and II. McGraw-Hill Book Company Inc, New York
64. Nasirpour F, Kapoor SG, Wu SM (1978) Runway roughness characterization by DDS approach. *J Transp Eng ASCE* 104(TE2):213–226
65. Newland DE (1986a) General theory of vehicle response to random road roughness, random vibration—status and recent developments, Elishakoff I and Lyon RH (eds.), Amsterdam: Elsevier
66. Newland DE (1986) The effect of a footprint on perceived surface roughness. *Proc Roy Soc (London) A* 405:303–327
67. Newland DE (1993) An introduction to random vibration, spectral and wavelet analysis, 3rd edn. Longman, New York
68. Nigam NC, Narayanan S (1994) Applications of random vibrations. Narosa Publishing House, New Delhi
69. Orr LW (1988) Truck pavement factors—the truck manufacturer's viewpoint. *Transc. SAE SP-765 881842:1–4*
70. Pan G, Atluri SN (1995) Dynamic response of finite sized elastic runways subjected to moving loads: a coupled bem/fem approach. *Int J Numer Methods Eng* 38(18):3143–3166
71. Pan T, Sun L (2012) Sub-microscopic phenomena of metallic corrosion studied by a combined photoelectron spectroscopy in air (PESA) and scanning Kelvin probe force microscopy (SKPFM) approach. *Int J Electrochem Sci* 7:9325–9344
72. Pan T, Sun L, Yu Q (2012) An atomistic-based chemophysical environment for valuating asphalt oxidation and antioxidants. *J Mol Model* 18:5113–5126. doi:10.1007/s00894-012-1512-2
73. Parkhilovskii IG (1968) Investigation of the probability characteristics of the surface of distributed types of roads. *Avtom Prom* 8:18–22
74. Payton RG (1964) An application of the dynamic Betti-Rayleigh reciprocal theorem to moving-point loads in elastic media. *Quart Appl Math* 21:299–313
75. Rauhut JB, Kennedy TW (1982) Characterizing fatigue life for asphalt concrete pavements, Transportation Research Record No. 888, Transportation Research Board
76. Road surface profile—reporting measured data (1984) Draft proposal ISO/DP 8608, mechanical vibration, international organization for standardization
77. Robson JD (1978) The role of Parkhilovskii model in road description. *Veh Systm Dyn* 7:153–162
78. Robson JD, Dodds CJ (1970) The response of vehicle components to random road surface indications. *Proc. IUTAM Symp., Frankfurt. (ORDER): Academic*
79. Sayer MW, Gillespie TD and Queiroz CAV (1986) The international road roughness experiment—establishing correlation and calibration standard for measurements. World Bank Tech. Paper No. 45, World Bank, Washington, DC, 25–29
80. Sayers MW (1985) Characteristic power spectral density functions for vertical and roll components of road roughness. *Proc. symp. on simulation control of ground vehicles and transp. Systems, ASME, New York*
81. Sayles RS, Thomas TR (1978) Surface topography as a non-stationary random process. *Nature* 271:431–434
82. Snyder JE, Wormley DN (1977) Dynamic interactions between vehicles and elevated, flexible randomly irregular guideways. *Transactions of the American Society of Mechanical Engineers. J Dyn Syst Meas Control* 99:23–33
83. Sobczyk K and Macvean DB, (1976). Non-stationary random vibration of road vehicles with variable velocity. Symposium on stochastic problems in dynamics, University of Southampton, England, (editor Clarkson BL)
84. Spiegel MB (1971) Theory and problems of advanced mathematics for engineers and scientists. McGraw-Hill Book Company, New York
85. Steele CR (1967) The finite beam with a moving load. *J Appl Mech, ASME* 34(2):111–118
86. Strathdee J, Robinson WH, Haines EM (1991) Moving loads on ice plates of finite thickness. *J Fluid Mech* 226:37–61
87. Sun L, Deng X, (1995) Dynamic loads caused by vehicle-pavement interactions, *J Southeast Univ*, 26(5): 142–145; also in *Proc. China Forum 95 on Transportation, Chongqing University, (Chongqing, Sichuan, China), 862–868 (in Chinese)*

88. Sun L (1998) Theoretical investigation on dynamics of vehicle–pavement interaction. Final Technical Report prepared for the National Science Foundation, Southeast University, Nanjing, China
89. Sun L (2001) A closed-form solution of Bernoulli–Euler beam on viscoelastic foundation under harmonic line loads. *J Sound Vib* 242(4):619–627
90. Sun L (2001) Closed-form representation of beam response to moving line loads. *J Appl Mech, ASME* 68(2):348–350
91. Sun L (2001) Computer simulation and field measurement of dynamic pavement loading. *Math Comput Simul* 56(3):297–313
92. Sun L (2001) Developing spectrum-based models for international roughness index and present serviceability index. *J Transp Eng ASCE* 127(6):463–470
93. Sun L (2001) Dynamic response of beam-type structures to moving line loads. *Int J Solids Struct* 38(48–49):8869–8878
94. Sun L (2001) On human perception and evaluation to road surfaces. *J Sound Vib* 247(3):547–560
95. Sun L (2001) Time-harmonic elastodynamic Green’s function of plates for line loads. *J Sound Vib* 246(2):337–348
96. Sun L (2002) A closed-form solution of beam on viscoelastic subgrade subjected to moving loads. *Comput Struct* 80(1):1–8
97. Sun L (2002) Optimum design of road-friendly vehicle suspension systems subject to rough road surface. *Appl Math Model* 26(5):635–652
98. Sun L (2002) Time-frequency analysis of thin slabs subjected to dynamic ring loads. *Acta Mechanica Nos* 153(3–4):207–216
99. Sun L (2003) An explicit representation of steady state response of a beam resting on an elastic foundation to moving harmonic line loads. *Int J Numer Anal Methods Geomech* 27:69–84
100. Sun L (2003) Dynamic response of Kirchhoff plate on a viscoelastic foundation to harmonic circular loads. *J Appl Mech, ASME* 70(4):595–600
101. Sun L (2003) Simulation of pavement roughness and IRI based on power spectral density. *Math Comput Simul* 61:77–88
102. Sun L (2005) Dynamics of plate generated by moving harmonic loads. *J Appl Mech, ASME* 72(5):772–777
103. Sun L (2006) Analytical dynamic displacement response of rigid pavements to moving concentrated and line loads. *Int J Solids Struct* 43:4370–4383
104. Sun L (2007) Steady-state dynamic response of a Kirchhoff’s slab on viscoelastic Kelvin’s foundations to moving harmonic loads. *J Appl Mech, ASME* 74(6):1212–1224
105. Sun L and Deng X (1996). Roughness and spectral analysis of runway profile. *Eastern China Highway, No. 2* (in Chinese)
106. Sun L, Deng X (1996) Analysis of pavement wave-number spectral density and random dynamic pressure generated by vehicle–pavement interactions. *J Xi’an Highw Univ* 16(2):17–21 (in Chinese)
107. Sun L, Deng X (1996) General theory for steady dynamic problem of infinite plate on an elastic foundation. *Acta Mech Sin* 28(6):756–760 (in Chinese)
108. Sun L, Deng X (1996) Mathematical model and experiment design of pavement dynamic loads. *J Xi’an Highw Univ* 16(4):50–53
109. Sun L, Deng X (1996) Mathematical model of weight in evaluation systems. *J Southeast Univ* 12(2):111–118 (in Chinese)
110. Sun L, Deng X (1996) Random pressure generated by airplane-airfield interactions. *J Chongqing Jiaotong Inst* 15(4):14–20 (in Chinese)
111. Sun L, Deng X (1996) Spectral analysis about surface evenness of airport pavement. *East China Highw* 2:35–38 (in Chinese)
112. Sun L, Deng X (1997) Transient response for infinite plate on Winkler foundation by a moving distributed load. *Chin J Appl Mech* 14(2):72–78 (in Chinese)
113. Sun L, Deng X (1997) Steady response of infinite plate on viscoelastic Kelvin foundation to moving loads. *Chin J Geotech Eng* 19(2):14–22 (in Chinese)
114. Sun L, Deng X (1997) Random response of beam under a moving random load in the line source form. *Acta Mech Sin* 29(3):365–368
115. Sun L, Deng X (1997) Influence of velocity, frequency and characteristics of vehicle on dynamic pavement loads. *China Civ Eng J* 30(6):137–147 (in Chinese)
116. Sun L, Deng X (1997) Random response of beam under a moving random load in the line source form. *Acta Mech Sin* 29(3):365–368 (in Chinese)
117. Sun L, Deng X (1997) Transient response for infinite plate on Winkler foundation by a moving distributed load. *Chin J Appl Mech* 14(2):72–78 (in Chinese)
118. Sun L, Deng X (1997) Transient response of bridge to traveling random vehicle loads. *J Vib Shock* 16(1):62–68 (in Chinese)
119. Sun L, Deng X (1997) Weight analysis in evaluation system. *J Syst Sci Syst Eng (English Edition)* 6(2):137–147
120. Sun L, Deng X (1997) Steady response of infinite plate on viscoelastic Kelvin foundation to moving loads. *Chin J Geotech Eng* 19(2):14–22 (in Chinese)
121. Sun L, Deng X (1998) Dynamic analysis of infinite beam under the excitation of moving line loads. *Appl Math Mech* 19(4):367–373 (in Chinese)
122. Sun L, Deng X (1998) Dynamic analysis of infinite beam under the excitation of moving line loads. *Appl Math Mech* 19(4):367–373 (in Chinese)
123. Sun L, Deng X (1998) Predicting vertical dynamic loads caused by vehicle–pavement interaction. *J Transp Eng, ASCE* 126(5):470–478
124. Sun L, Deng X (1998) Predicting vertical dynamic loads caused by vehicle–pavement interaction. *J Transp Eng, ASCE* 124(5):470–478
125. Sun L, Deng X (1998) Recent advances on spectral analysis of pavement surface. *J Southeast Univ* 14(4):223–234 (in Chinese)
126. Sun L, Duan Y (2013) Dynamic response of top-down cracked asphalt concrete pavement under a half-sinusoidal impact load. *Acta Mechanica*. doi:10.1007/s00707-013-0849-7
127. Sun L, Greenberg B (1999) Dynamic response of linear systems to moving stochastic sources. *J Sound Vib* 229(4):957–972
128. Sun L, Greenberg BS (2000) Dynamic response of linear systems to moving stochastic sources. *J Sound Vib* 229(4):957–972
129. Sun L, Gu W (2011) Pavement condition assessment using fuzzy logic theory and analytic hierarchy process. *J Transp Eng ASCE* 137(9):648–655
130. Sun L, Kennedy TW (2002) Spectral analysis and parametric study of stochastic pavement loads. *J Eng Mech, ASCE* 128(3):318–327
131. Sun L, Luo F (2007) Arrays of dynamic circular loads moving on an infinite plate. *Int J Numer Meth Eng* 71(6):652–677
132. Sun L, Luo F (2007) Nonstationary dynamic pavement loads generated by vehicles traveling at varying speed. *J Transp Eng, ASCE* 133(4):252–263
133. Sun L, Luo F (2008) Steady-state dynamic response of a Bernoulli–Euler beam on a viscoelastic foundation subject to a platoon of moving dynamic loads. *J Vib Acous, ASME* 130(5):051002.1–051002.19
134. Sun L, Luo F (2008) Transient wave propagation in multilayered viscoelastic media—theory, numerical computation and validation. *J Appl Mech, ASME* 75(3):031007.1–031007.15
135. Sun L, Ronald Hudson W (2005) Probabilistic approaches for pavement fatigue cracking prediction based on cumulative damage using Miner’s law. *J Eng Mech, ASCE* 131(5):546–549
136. Sun L, Su J (2001) Modeling random fields of road surface irregularities. *Int J Road Mater Pavement Des* 2(1):49–70

137. Sun L, Wang Dengzhong (2012) Nondestructive testing and evaluation of subgrade compaction by portable falling deflectometer. *J Highw Transp Res Dev* 29(2):41–47 (in Chinese)
138. Sun L, Xin Xiantao GuW (2012) Comprehensive comparison of nano-materials for asphalt modification. *J Transp Eng Inf* 10(2):1–11 (in Chinese)
139. Sun L and Zheng KA (1998) Unified theory for solving moving source problem: general principle of the Duhamel integral, *Academic Periodical Abstracts of China*, Vol. 4, No. 4 (in Chinese)
140. Sun L, Zheng K (1998) Distress stress analysis of flexible pavement structure. *J Chongqing Jiaotong Inst* 17(4):1–7 (in Chinese)
141. Sun L, Zhu YT (2013) A two-stage serial viscoelastic-viscoplastic constitutive model for characterizing nonlinear time-dependent deformation behavior of asphalt mixtures. *Constr Build Mater* 40:584–595
142. Sun L, Deng X, Zhang J (1996) An optimal method for interchange design. *East China Highw* 3:27–31 (in Chinese)
143. Sun L, Deng X, Gu W (1997) Identification of typical asphalt pavement structures for category design of pavements. *China Civ Eng J* 30(3):55–62 (in Chinese)
144. Sun L, Deng X, Gu W (1997) Recent advancement of pavement roughness and dynamic loads—I. Pavement spectral analysis and its application, II. Theory and experiment of pavement dynamic loads. *Acad Period Abstr China* 3(12):1442–1443 (in Chinese)
145. Sun L, Deng X, Gu W (1998) Random response of Kirchhoff plate and Bernoulli–Euler beam under moving random loads. *Acad Period Abstr China* 4(1):127 (in Chinese)
146. Sun L, Deng X, Gu W (1998) Steady and transient response of infinite plate on Kelvin foundation generated by a moving distributed load. *Acad Period Abstr China* 4(1):126 (in Chinese)
147. Sun L, Zhang Z, Ruth J (2001) Modeling indirect statistics of surface roughness. *J Transp Eng, ASCE* 127(2):105–111
148. Sun L, Hudson WR, Zhang Z (2003) Empirical-mechanistic method based stochastic modeling of fatigue damage to predict flexible pavement fatigue cracking for transportation infrastructure management. *J Transp Eng ASCE* 129(2):109–117
149. Sun L, Luo F, Chen TH (2005) Transient response of a beam on viscoelastic foundation under impact loads during nondestructive testing. *J Earthq Eng Eng Vib* 4(2):325–333
150. Sun L, Cai X, Yang J (2006) Genetic algorithm-based optimum vehicle suspension design using minimum dynamic pavement load as a design criterion. *J Sound Vib* 301(1–2):18–27
151. Sun L, Kenis W, Wang W (2006) Stochastic spatial excitation induced by a distributed contact with homogenous Gaussian random fields. *J Eng Mech, ASCE* 132(7):714–722
152. Sun L, Gu W, Luo F (2009) Steady state response of multilayered viscoelastic media under a moving dynamic distributed load. *J Appl Mech, ASME* 75(4):0410011–04100115
153. Sun L, Gu W, Mahmassani H (2011) Estimation of expected travel time using moment approximation. *Can J Civ Eng* 38:154–165
154. Sun L, Li A, Zhang Y, Xin X, Shao J (2011) Study on gradation of cement-fly ash stabilized coal gangue. *J Transp Eng Inf (in Chinese)* 9(4):7–10
155. Sun L, Luo F, Gu W (2011) Elastodynamic inversion of multilayered media via surface deflection—Part I: methodologies. *J Appl Mech* 78(5):2323–2333
156. Sun L, Wang D, Zhang H (2012) Predictive models of subgrade deflection using data from portable falling weight deflectometer. *J Southeast Univ* 42(5):970–975 (in Chinese)
157. Sun L, Xin X, Wang H, Gu W (2012) Microscopic mechanism of modified asphalt by multi-dimensional and multi-scale nanomaterial. *J Chin Ceram Soc* 40(10):1437–1447 (in Chinese)
158. Sun L, Xin X, Wang H, Gu W (2012) Performance of nano-material modified asphalt as paving materials. *J Chin Ceram Soc* 40(8):1095–1101
159. Sun L, Pan Y, and Gu W (2013) High order thin layer method for viscoelastic wave propagation in stratified media, *Comput Methods Appl Mech Eng*, 256, 65–76. <http://www.sciencedirect.com/science/article/pii/S0045782513000157>. Accessed 17 Sep 2013
160. Sun L, Chen L and Gu W (2013) Stress and deflection parametric study of high-speed railways CRTS-II Blastless Track Slab on bridge foundation. *ASCE J Transp Eng* (in press)
161. Sun L, Gu W and Xu B (2013) Characterizing uncertainty in pavement performance prediction using Monte Carlo simulation. *J Southeast Univ, (English Edition)* (in press)
162. Sun L, You K, Wang D, Gu W (2013) A study on the influence of road conditions on vehicle rollover. *J Southeast Univ (in press)* (in Chinese)
163. Sun L, Zhu H, Wang H, Gu W (2013) Preparation of nano-modified asphalt and its road performance evaluation. *China J Highw Transp* 26(1):1–8 (in Chinese)
164. Sun L, Zhu H, Zhu Y (2013) A two-stage viscoelastic-viscoplastic damage constitutive model of asphalt mixtures. *J Mater Civ Eng ASCE*. doi:10.1061/(ASCE)MT.1943-5533.0000646
165. Sussman NE (1974) Statistical ground excitation model for high speed vehicle dynamic analysis. *High Speed Ground Transp J* 8:145–154
166. Sweatman PF (1983) A study of dynamic wheel forces in axle group suspensions of heavy vehicles, Special Report No. 27, Australia Road Research Board
167. Van Deusen BD and McCarron GE (1967) A new technique for classifying random surface roughness: *Trans. SAE* 670032, Society of Automotive Engineers, New York
168. Wang SY, Sun L, Tang CA, Yang TH (2009) Numerical study of hydraulic fracture initiation and propagation around injection cavity in stiff soil. *Constr Build Mater* 23(6):2196–2206
169. Wang SY, Sun L, Zhu WC, Tang CA (2013) Numerical study on static and dynamic fracture evolution around rock cavities. *J Rock Mech Geotech Eng* 5(3):970–975
170. Wells VL, Han Y (1995) Acoustics of a moving source in a moving medium with application to propeller noise. *J Sound Vib* 184(4):651–663
171. Woodrooffe and Leblanc PA (1986) The influence of suspension variations on dynamic wheel loads of heavy vehicles. *SAE Technical Paper No. 861973*, Society Automotive Engineers
172. Yadav D, Nigam NC (1978) Ground induced non-stationary response of vehicles. *J Sound Vib* 106(2):217–225
173. You K, Sun L, Gu W (2010) Quantitative assessment of roadside safety on mountain highway. *J Transp Eng Inf* 8(3):49–55
174. You K, Wu J, Sun L, Zhang H (2011) Influence of road geometry on vehicle handling stability. *J Highw Transp Res Dev* 28(10):109–117 (in Chinese)
175. You K, Sun L, Gu W (2012) Risk analysis-based identification of road hazard locations using vehicle dynamic simulation. *J Southeast Univ* 42(1):150–155 (in Chinese)
176. You K, Sun L, Gu W (2012) Reliability-based risk analysis of roadway horizontal curve. *J Transp Eng, ASCE* 138(8):1071–1081. doi:10.1061/(ASCE)TE.1943-5436.0000402
177. You K, Sun L and Gu W (2013) Reliability design of highway horizontal curve based on vehicle stability analysis. *J Traffic Transp Eng*, (in press) Chinese
178. Zhu WQ (1992) *Random vibration*. Academic Press, Beijing (in Chinese)
179. Zhu H, Sun L (2013) A viscoelastic-viscoplastic damage constitutive model for asphalt mixture based on thermodynamics. *Int J Plast* 40:81–100

180. Zhu HR and Sun L (2013) A mechanistic predictive model of rutting based on a two-stage serial viscoelastic-viscoplastic damage constitutive model for asphalt mixtures. *J Eng Mech, ASCE*, (in press)
181. Zhu Y, Wang Y, Sun L, You K (2009) Thermodynamic formulations of different coupling conditions between damage and plasticity. *J Southeast Univ* 39(5):39–65 (in Chinese)
182. Zhu H, Sun L, Yang J, Chen Z (2011) Developing master curves and predicting dynamic modulus of polymer modified asphalt mixtures. *J Mater Civ Eng, ASCE* 23(131):9–19
183. Zhu Y, Sun L, Xu HL (2011) L-curve based Tikhonov's regularization method for determining relaxation modulus from creep test. *J Appl Mech, ASME* 78(2):031002
184. Zhu Y, Sun L, Zhu H, Yu Q (2013) Time-dependent constitutive model of asphalt mixtures based on constant strain rate tests. *J Wuhan Univ Technol* (in Chinese) 36(5):922–926
185. Zhu H, Sun L and Zhu Y (2013) A viscoelastic-viscoplastic damage constitutive model based on thermodynamics theory for asphalt mixtures. *Chin J Highw Eng*, 26(1) (in Chinese)
186. Zhu Y, Sun L, Zhu H, Xiang W (2013) A constitutive model of viscoelastic-viscoplastic solids based on thermodynamics theory. *Chin Quart J Mech*, 31(4) (in Chinese)
187. Zu JWZ, Han RPS (1994) Dynamic response of a spinning Timoshenko beam with general boundary conditions and subjected to a moving load. *J Appl Mech, ASME* 61(1):152–160